MYBL2 regulates ATM to control replication initiation and prevent replication stress in pluripotent stem cells

Daniel Blakemore[1], Nuria Vilaplana[1], Ruba Almaghrabi[1], Elena Gonzalez[1], Miriam Moya[1], Carl Ward[2,3], George Murphy[4], Agnieszka Gambus[1], Eva Petermann[1], Grant S. Stewart[1,5], Paloma García[1,5*]

[1]Institute of Cancer and Genomic Science, College of Medical and Dental Sciences, University of Birmingham, UK;

[2]Laboratory of Integrative Biology, Guangzhou Institutes of Biomedicine and Health, Chinese Academy of Sciences (CAS), Guangzhou, China. [3] Chinese Academy of Sciences (CAS), Key Laboratory of Regenerative Bology and Guangdong Provincial Key Laboratory of Stem Cell and regenerative Medicine, Guangzhou Institutes of Biomedicine and Health, Guangzhou, 510530, China. [4]Department of Medicine, Boston University School of Medicine, Boston, Massachusetts, USA.

[5]Co-senior authors

*** Corresponding author p.garcia@bham.ac.uk**

Summary

Replication stress, a major cause of genome instability in cycling cells, is mainly prevented by the ATR-dependent replication stress response pathway in somatic cells. However, the replication stress response pathway in embryonic stem cells (ESCs) may be substantially different due to alterations in cell cycle phase length. The transcription factor MYBL2, which is implicated in cell cycle regulation, is expressed between hundred to thousand-fold more highly in ESCs compared to somatic cells. Here we show that MYBL2 functions to activate ATM and suppress replication stress in ESCs. Consequently, loss of MYBL2 or inhibition of ATM or Mre11 in ESCs, results in replication fork slowing, increased fork stalling and elevated origin firing. Additionally, we demonstrate that inhibition of CDC7 activity rescues replication stress induced by MYBL2 loss and ATM inhibition, suggesting that uncontrolled new origin firing may underlie the replication stress phenotype resulting from loss/inhibition of MYBL2 and ATM. Overall, this study proposes that in addition to ATR, a MYBL2-MRN-ATM replication stress response pathway functions in ESCs to control DNA replication initiation and prevent genome instability.

Introduction

DNA replication is a highly complex process that requires tight regulation to ensure that genome stability is maintained. Obstacles to DNA replication activate the replication stress response pathway, which not only functions to ensure that the initiation of DNA replication and progression through the cell cycle progression are suppressed, but also acts to facilitate the repair and restart of damaged replication forks (Aguilera and Gomez-Gonzalez, 2008; Bartek et al., 2004) (Zeman and Cimprich, 2014).

Two main serine/threonine protein kinases are responsible for controlling the cellular response to genetic damage and impedements to DNA replication: ataxia-telangiectasia mutated (ATM) and ataxia-telangiectasia and Rad3 related (ATR). ATR is activated following its recruitment to RPA coated ssDNA, a common intermediate the occurs during normal DNA replication and also as a consequence of replication stress. It has been shown that ATR is essential for the survival of proliferating cells as its loss is embryonic lethal (de Klein et al., 2000). In contrast, ATM is recruited by the MRN complex to DNA ends and is primarily associated with signalling the presence of DNA double-strand breaks (DSB) (Bakkenist and Kastan, 2003; Khanna et al., 2001; Valerie and Povirk, 2003). Activation of the ATR kinase during replication leads to the phosphorylation and activation of the CHK1 kinase, which functions to suppress new replication origin firing (Guo et al., 2000; Liu et al., 2000; Moiseeva et al., 2019), promote fork stability and prevent premature entry into mitosis (Cimprich and Cortez, 2008). In contrast, it is thought that ATM is activated during S-phase only upon MRN-dependent recruitment to sites of DSBs i.e. collapsed replication forks (Bakkenist and Kastan, 2003; Lee and Paull, 2004). However, various studies have challenged this canonical pathway for ATM activation by demonstrating that its recruitment and activity is dependent upon chromatin context, indicating that ATM may be capable of being activated in the absence of DSBs (Bakkenist and Kastan, 2003; Bencokova et al., 2009; Cam et al., 2010; Ewald et al., 2008; Iwahori et al., 2014; Olcina et al., 2010; Olcina et al., 2013). Furthermore, studies performed in *Xenopus laevis* egg extracts have indicated a specific role for ATM in regulating the timing of replication (Marheineke and Hyrien, 2004; Shechter et al., 2004). Therefore, it has been hypothesised that ATM could have additional roles in replication control, specifically in non-somatic cell types.

In embryonic stem cells (ESC), safeguarding genome stability during DNA replication is of extreme importance as alterations to the genome will be transmitted to their differentiated daughter cells during development, potentially compromising tissue integrity and function. ESCs proliferate very rapidly and possess an atypical cell cycle with short GAP phases and a weak G1-S checkpoint (Ballabeni et al., 2011; Coronado et al., 2013; Kapinas et al., 2013;

Savatier et al., 1994). It has been suggested that mESCs may contain a significant fraction of unreplicated DNA as they enter mitosis (Ahuja et al., 2016). Nevertheless, despite these traits, pluripotent stem cells actually have a very low mutation rate (Cervantes et al., 2002; Fujii-Yamamoto et al., 2005; Kapinas et al., 2013) and maintain genome stability more efficiently than somatic cell types (Ahuja et al., 2016; Kapinas et al., 2013; Murga et al., 2007; Zhao et al., 2015). However, how these cells retain such a low mutational rate in the presence of high levels of endogenous replication stress is still not properly understood.

One protein that is unusually highly expressed in ESCs and key for genome stability is the transcription factor MYBL2 (alias, B-MYB) (Lorvellec et al., 2010; Sitzmann et al., 1996; Tarasov et al., 2008). Similar to ATR, targeted disruption of MYBL2 leads to early embryonic lethality (Tanaka et al., 1999). MYBL2 has been shown to be important for transactivating the promoters of genes responsible for regulating the G2/M transition (Knight et al., 2009; Lorvellec et al., 2010; Osterloh et al., 2007; Tarasov et al., 2008; Wolter et al., 2017). More specifically, the MuvB core cooperates with MYBL2 to recruit FOXM1 to the promoters of specific genes, such as Cyclin B, survivin and CDC25 phosphatase, which are responsible for mediating G2–M checkpoint control (Down et al., 2012; Lefebvre et al., 2010; Martinez and Dimaio, 2011; Sadasivam and DeCaprio, 2013; Sadasivam et al., 2012). In addition to this, a recent study identified a signalling axis, involving ATR-CDK1-FOXM1 and demonstrated that it cooperates with MYBL2 to govern the proper exit from S-phase into G2 (Saldivar et al., 2018). Moreover, it has also been shown that YAP, a component of the HIPPO signalling pathway, interacts with the MYBL2-MuvB complex to influence the expression of genes important for mitosis (Pattschull et al., 2019). Whilst the ability of MYBL2 to act as a transcription is critical for cell cycle regulation, our previous work in ESCs has highlighted the importance of MYBL2 for maintaining normal replication fork progression under unperturbed conditions, as stem cells lacking MYBL2 displayed a significantly reduction in replication fork speed (Lorvellec et al., 2010). However, whether this replication phenotype is caused by dysfunction of the ATR-CDK1-FOXM1 axis or aberrant regulation of YAP-dependent gene transcription remains unknown. Here, we demonstrate that the replication stress caused by loss of MYBL2 in ESCs is epistatic with loss of Mre11 or ATM function and can be rescued by suppressing origin firing via inhibition of CDC7. This suggests that uncontrolled replication initiation underlies the replication stress phenotype exhibited by cells lacking MYBL2 and that it is not caused by alterations in the expression of genes involved in controlling the cell cycle. Taken together, this work identifies ATM as a critical regulator of origin firing in pluripotent stem cells and highlights the importance of MYBL2-ATM in controlling the initiation of origin firing and the replication stress response in these cells.

Results

Mybl2$^{\Delta/\Delta}$ ESCs display a replication stress phenotype characterized by a decrease in replication fork speed and an increase in replication fork instability.

Consistent with our previous work (Lorvellec et al., 2010), DNA fibre analysis revealed that replication fork progression was significantly reduced in *Mybl2*$^{\Delta/\Delta}$ ESCs compared to a WT counterpart, with a 65% reduction in the median replication fork speed (Figure 1A and EV1A). Analysis of the relative percentage of different replication structures revealed a notable decrease in the percentage of elongating forks in the *Mybl2*$^{\Delta/\Delta}$ ESCs compared to *Mybl2*$^{+/+}$ ESCs (Figure EV1B and EV1C). This reduction in actively elongating replication fork structures was associated with an increase in fork stalling and new origin firing, the latter of which is a known compensation mechanism invoked to counteract a reduction in the cellular replicative capacity (Figure EV1D and EV1E).

To further investigate potential changes in the kinetics of replication fork progression, the ratio of first and second label replication tracks of elongating forks was calculated as a measure of replication fork stability (Maya-Mendoza et al., 2018). An increase in the ratio with respect to wild type cells suggests a disruption of continuous fork progression due to increased fork instability. Notably, the *Mybl2*$^{\Delta/\Delta}$ ESCs exhibited a significant increase in replication fork instability compared to *Mybl2*$^{+/+}$ ESCs (Figure 1B). In keeping with this observation, *Mybl2*$^{\Delta/\Delta}$ ESCs also displayed a strong asymmetry phenotype of newly fired replication forks initiating from the same origin when compared to *Mybl2*$^{+/+}$ ESCs (Figure 1C). This indicates that MYBL2 plays a critical role in maintaining replication fork stability in the absence of exposure to any exogenous genotoxins.

It is known that prolonged replication stress leads to the formation of ultra-fine bridges (UFBs) between separating sister chromatids in anaphase due to the presence of under-replicated DNA (Chan et al., 2018). To investigate whether loss of MYBL2 leads to increased UFBs, immunofluorescence staining using an antibody to PICH, a DNA translocase known to coat ultra-fine bridges during anaphase (Baumann et al., 2007; Chan and Hickson, 2011) was carried out on asynchronous *Mybl2*$^{+/+}$ and *Mybl2*$^{\Delta/\Delta}$ ESCs. In the *Mybl2*$^{+/+}$ ESCs, 20% of anaphases exhibited UFBs, which is comparable to levels previously observed for normal stem cells (Broderick et al., 2015; Hengeveld et al., 2015; Saldivar et al., 2018). Strikingly, there was a significant increase (60%) in the percentage of UFB positive anaphases in the *Mybl2*$^{\Delta/\Delta}$ compared to *Mybl2*$^{+/+}$ ESCs (Figure 1D). Overall, these data build upon our

previous findings and strongly demonstrate that MYBL2 loss in ESCs culminates in chronic replication stress leading to under-replicated DNA passing into mitosis.

Mybl2$^{\Delta/\Delta}$ ESCs exhibit increased replication-associated genome instability

Cells under chronic replication stress exhibit elevated levels of DNA damage that can be partly attributed to an increase in stalled forks, which if left unresolved, are vulnerable to collapse into double strand breaks (DSBs) (Petermann et al., 2010; Zeman and Cimprich, 2014). Therefore, to determine whether the increased replication stress present in MYBL2 deficient ESCs resulted in more replication-associated DNA breakage, total DNA breaks were quantified using an alkaline comet assay (Ostling and Johanson, 1984; Singh et al., 1988). Exposure of cells to camptothecin (CPT), a genotoxic agents known to induce replication-associated DNA breakage was used a positive control. Notably, the *Mybl2*$^{\Delta/\Delta}$ ESCs exhibited significantly increased levels of spontaneous DNA breakage as measured by the average olive tail moment (OTM) when compared to the *Mybl2*$^{+/+}$ ESCs (Figure 1E and 1F). Whilst the exposure of ESCs to CPT elevated the DNA breakage to a level that was not significantly different between the two genotypes.

To ascertain whether the increase in OTM in *Mybl2*$^{\Delta/\Delta}$ ESCs was due to DSB formation during replication, immunofluorescence was performed using 53BP1 and EdU as markers of DSBs and cells in S-phase respectively. Again, exposure to CPT was used as a positive control for replication-associated DNA breakage. We observed a two-fold increase in the percentage of S-phase nuclei displaying more than six 53BP1 foci in *Mybl2*$^{\Delta/\Delta}$ cells (EdU positive) when compared to the *Mybl2*$^{+/+}$ ESCs (Figure 1G and Appendix Figure S1). As expected, in response to CPT treatment, both the *Mybl2*$^{+/+}$ and *Mybl2*$^{\Delta/\Delta}$ ESCs exhibited a large increase in the percentage of cells with over six 53BP1 foci. These findings suggest that the increased spontaneous DNA damage in the *Mybl2*$^{\Delta/\Delta}$ ESCs most likely arises as a consequence of replication fork collapse.

Mybl2$^{\Delta/\Delta}$ ESC fail to activate the DNA damage-activated, G2/M cell cycle checkpoint

Given that *Mybl2*$^{\Delta/\Delta}$ ESCs show signs of chronic replication stress (Figure 1A-C) leading to unreplicated DNA (Figure 1D) and DNA breakage (Figure 1E-F), it would be expected that these cells would arrest in S- or G2-phase of the cell cycle due to prolonged activation of the DNA damage checkpoint response (Zeman and Cimprich, 2014). Interestingly however, *Mybl2*$^{\Delta/\Delta}$ ESCs still retain the capacity to proliferate even in the presence of DNA damage. Since MYBL2 has been shown to regulate the transcription of genes linked with cell cycle regulation (Henrich et al., 2017; Katzen et al., 1998; Sadasivam et al., 2012; Saldivar et al., 2018; Tarasov et al., 2008), we hypothesised that the capacity of the *Mybl2*$^{\Delta/\Delta}$ cells to

continue cycling in the presence of replication stress and DNA damage could be attributed to deregulation of the DNA damage cell cycle checkpoints. To investigate this, *Mybl2*$^{+/+}$ and *Mybl2*$^{\Delta/\Delta}$ cells were treated with CPT and then DNA fibre analysis was used to monitor the DNA damage-induced suppression of new origin firing as a marker of activation of the intra-S phase checkpoint. Unexpectedly, we did not observe a reduction in new origin firing following exposure to CPT in *Mybl2*$^{+/+}$ ESCs, rather, the level of new origin firing increased. In ESCs lacking MYBL2, CPT treatment had no observable affect on the already high level of new origin firing (Figure 2A). This suggests that like the G1/S-phase checkpoint, murine ESCs do not retain the capacity to activate the DNA damage-induced intra-S phase checkpoint and that the observed increase in new origin firing following exposure to CPT represents an adaptive response of the cell to trigger more origin firing when faced with high levels of replication stress. In keeping with this, CPT treatment resulted in a significant slowing of DNA replication in *Mybl2*$^{+/+}$ ESCs, which was comparable to the replication rate of untreated *Mybl2*$^{\Delta/\Delta}$ ESCs (Figure 2B). Interestingly, the slow rate of replication of the *Mybl2*$^{\Delta/\Delta}$ ESCs was unaffected by exposure to CPT, indicating that the compromised rate of replication is sufficient to prevent any significant collisions between replication machinery and CPT-induced abortive Top1 complexes.

To assess whether ESCs were also incapable of activating the G2/M DNA damage checkpoint, again *Mybl2*$^{+/+}$ and *Mybl2*$^{\Delta/\Delta}$ cells were treated with CPT and then the percentage of cells passing into mitosis in the presence of DNA damage was quantified using histone H3 phosphorylated on serine-10 (H3-pS10) as a marker of mitotic cells. To prevent cells traversing through mitosis, cells were treated also with colcemid, a tubulin depolymerising agent which arrests cells in metaphase (Figure 2C) (Li et al., 2005). As expected, robust activation of the G2/M checkpoint by CPT was induced in the *Mybl2*$^{+/+}$ ESCs as measured by a significant reduction in H3-pS10 positive cells (from 23.3% to 4.5%). Interestingly, exposure of *Mybl2*$^{\Delta/\Delta}$ ESCs to CPT failed to induce a significant reduction in H3-pS10 positive cells, indicative of an inability to activate the DNA damage-induced G2/M checkpoint (Figure 2C). These data are consistent with the role of Mybl2 in regulating the G2-M transition in the presence of DNA damage.

A critical event facilitating the ability of cells to activate the G2/M checkpoint is the WEE1-dependent phosphorylation of CDK1 on tyrosine-15 (Tyr-15) (Heald et al., 1993; Watanabe et al., 1995). Therefore, to ascertain whether the G2/M checkpoint defect observed in the *Mybl2*$^{\Delta/\Delta}$ ESCs was caused by aberration regulation of CDK1, we utilised Western blotting to measure the levels of CDK1 Tyr-15 phosphorylation. Interestingly, this analysis revealed that *Mybl2*$^{\Delta/\Delta}$ ESCs exhibited reduced levels of CDK1 phosphorylated on Tyr-15 when compared

to *Mybl2*$^{+/+}$ ESCs, whilst no obvious variations in CDK1 protein levels were observed (Figure 2D). As expected, inhibition of the WEE1 kinase completely abolished phospho-CDK1 levels in both the *Mybl2*$^{+/+}$ and *Mybl2*$^{\Delta/\Delta}$ ESCs (Appendix Figure S2). To analyse the effect of additional stress upon CDK1 activity in the *Mybl2*$^{\Delta/\Delta}$ ESCs, cells were treated with CPT for 4 hours. Following CPT treatment, *Mybl2*$^{+/+}$ ESCs displayed an increase in the P-CDK1 (Tyr15) levels, presumably reflecting the inhibition of CDK1 activity by cell cycle checkpoint signalling. In contrast however, CPT-treated *Mybl2*$^{\Delta/\Delta}$ ESCs did not display any obvious increase in P-CDK1, consistent with these cells lacking this DNA damage-activated checkpoint response (Figure 2D). Overall, these data indicate that chronic loss of MYBL2 in ESCs results in abnormal CDK1 activity leading to a weaker G2/M cell cycle checkpoint.

Reduced CHK1 activation in MYBL2-ablated ESC after exposure to DNA damage

To investigate the underlying cause of the deregulated CDK1 activity in *Mybl2*$^{\Delta/\Delta}$ cells, we focused on CHK1, which is the principal checkpoint kinase acting downstream of ATR and known to be important for the suppression of origin firing and cell cycle checkpoint activation through its ability to inhibit CDK1 and CDK2 (Petermann et al., 2010). Western blotting analysis of CHK1 in unperturbed conditions showed that the level of phospho-CHK1(Ser345) in the *Mybl2*$^{\Delta/\Delta}$ ESCs was slightly increased compared to *Mybl2*$^{+/+}$ ESCs (Figure 3A), which is consistent with the increased spontaneous replication stress we have observed in these cells. Interestingly however, the level of P-CHK1 in the *Mybl2*$^{\Delta/\Delta}$ ESCs was significantly reduced when compared to *Mybl2*$^{+/+}$ ESCs following exposure to CPT, suggesting that *Mybl2*$^{\Delta/\Delta}$ ESCs can not efficiently activate CHK1 in response to certain types of genotoxic stress (Figure 3A).

To further investigate the mechanism of CHK1 activation in ESCs, cells were treated with either an ATR (AZ20) or ATM (KU60019) inhibitor for two hours before subjecting the cells to 5 Gy ionizing radiation to induce DNA damage. Consistent with our previous observation, *Mybl2*$^{\Delta/\Delta}$ ESCs failed to efficiently phosphorylate CHK1 after exposure to IR as compared to the WT ESCs (Figure 3B). Furthermore, as expected, treatment with the ATR inhibitor reduced the levels of P-CHK1 in the ESCs irrespective of genotype (Figure 3B). Interestingly however, treatment with the ATM inhibitor also appeared to reduce the levels of P-CHK1 in the *Mybl2*$^{+/+}$ but not the *Mybl2*$^{\Delta/\Delta}$, indicating not only the presence of crosstalk between ATR and ATM signalling pathways with respect to CHK1 activation in ESCs but also that a loss of MYBL2 compromises the ability of ATM to be activated (Figure 3B). Moreover, the increased levels of spontaneous P-CHK1 observed in the untreated *Mybl2*$^{\Delta/\Delta}$ ESCs were also reduced by the ATR inhibitor but not the ATM inhibitor (Appendix Figure S3). Altogether, our data

suggest that CHK1 activation is dependent on both ATR and ATM signalling and that MYBL2 may function upstream of ATM to activate CHK1.

Inhibition of ATR signalling results in severe replication stress independently of MYBL2

Since *Mybl2*$^{\Delta/\Delta}$ ESCs are unable to properly activate CHK1 in response to exogenous DNA damage, this suggests a potential role for MYBL2 in regulating the replication stress response downstream of ATM and possibly ATR. To determine whether MYBL2 acts in one or both of these replication stress response pathways, we utilised the ATR and ATM inhibitors to ascertain whether the endogenous replication stress observed in the *Mybl2*$^{\Delta/\Delta}$ ESCs was epistatic with inhibition of the activity of either one of these kinases.

Initially, *Mybl2*$^{+/+}$ and *Mybl2*$^{\Delta/\Delta}$ ESCs were treated with an ATR inhibitor for 1.5 hours before labelling active replication and performing DNA fibre analysis (Figure EV2A). In both the *Mybl2*$^{+/+}$ and *Mybl2*$^{\Delta/\Delta}$ ESCs, ATR inhibition resulted in a highly significant decrease in the speeds of replication fork progression (Figure 3C and EV2B-C). Interestingly however, the inhibition of ATR only de-regulated replication initiation in the *Mybl2*$^{+/+}$ but not the *Mybl2*$^{\Delta/\Delta}$ ESCs (Figure 3D and EV2D). To determine whether ATR inhibition affected fork stability, the ratio between the lengths of first- and second-labeled tracks of elongating forks was calculated. The average fork ratio in the *Mybl2*$^{+/+}$ ESCs treated with ATR inhibitor increased significantly when compared to that of untreated cells (Figure 3E and EV2D), whereas in contrast, fork instability only moderately increased in *Mybl2*$^{\Delta/\Delta}$ ESCs following treatment with the ATR inhibitor (Figure 3E and EV2D). Overall, these findings suggest that MYBL2 may function downstream of ATR to regulate the response to replication stress in ESCs but that loss of ATR has a much greater impact on replication fork stability and elongation rates than the loss of MYBL2.

ATM and MYBL2 function together to prevent replication stress and genome instability in pluripotent stem cells

Given the severity of the replication stress phenotype induced following ATR inhibition relative to that present in the *Mybl2*$^{\Delta/\Delta}$ ESCs, it is conceivable that either MYBL2 only functions within a subset of ATR-dependent responses to replication stress or acts within a parallel pathway that facilitates the ATR-dependent replication stress response i.e. a pathway regulated by ATM. Therefore, to further investigate a link between MYBL2 and ATM, *Mybl2*$^{+/+}$ and *Mybl2*$^{\Delta/\Delta}$ ESCs were treated with a chemical inhibitor of ATM before the addition of IdU and CldU to label actively replicating DNA (Figure 4A). DNA fibre analysis revealed that replication fork progression in the *Mybl2*$^{+/+}$ ESCs was surprisingly sensitive to

ATM inhibition, albeit not as sensitive to ATR inhibtion, with the median replication forks rate decreasing to levels similar to *Mybl2*$^{\Delta/\Delta}$ ESCs (Figure 4B). Interestingly, ATM inhibition in the *Mybl2*$^{\Delta/\Delta}$ ESCs had no additional effect upon replication forks progression rate (Figure 4B) indicating that the spontaneous replication stress present in the *Mybl2*$^{\Delta/\Delta}$ ESCs most likely arises as a consequence of a compromised ATM-dependent replication stress response pathway. Consistent with ATM and MYBL2 functioning in the same pathway, inhibition of ATM led to a significant increase in replication fork asymmetry and new origin firing in *Mybl2*$^{+/+}$ ESCs but not the *Mybl2*$^{\Delta/\Delta}$ ESCs (Figure 4C-D), which was not due to any alterations in cell cycle profile (Figure EV3). However, in keeping with ATR playing a predominant role in controlling the replication stress response in ESCs and ATM facilitating this, combined inhibition of ATR and ATM reduced replication rates in ESCs irrespective of genotype to levels comparable to those observed following inhibition of ATR alone (Figure EV2E).

To confirm that the treatment with ATM inhibitor was causing replication stress similar to that seen in the MYBL2$^{\Delta/\Delta}$ ESCs, the formation of UFBs following exposure to the ATM inhibitor was assessed. As expected, the *Mybl2*$^{+/+}$ ESCs treated with ATM inhibitor accumulated under-replicated DNA, as evidenced by the high percentage of cells displaying UFB positive anaphases (70%). Notably, ATM inhibition induced UFBs in *Mybl2*$^{+/+}$ ESCs at a level comparable to that observed in *Mybl2*$^{\Delta/\Delta}$ ESCs (Figure 4E). Next, we asked the question whether the DNA damage in the *Mybl2*$^{\Delta/\Delta}$ ESCs is mimicked by ATM inhibition in WT ESCs. To test this, *Mybl2*$^{+/+}$ and *Mybl2*$^{\Delta/\Delta}$ ESCs were treated with an ATM inhibitor before performing immunofluorescence staining for 53BP1 in cells also treated with EdU (Figure EV4A). Inhibition of ATM in the *Mybl2*$^{+/+}$ ESCs resulted in an increase in 53BP1 foci in EdU positive cells with a three-fold increase in the percentage of cells with more than six foci (Figure EV4B and EV4C). Interestingly, ATM inhibition in the *Mybl2*$^{\Delta/\Delta}$ had no additional effect upon the already elevated levels of 53BP1 recruitment (Figure EV4B and EV4C). Together, these data suggests that MYBL2 functions upstream of ATM in ESCs to suppress replication stress and genome instability. Based on this, we treated *Mybl2*$^{+/+}$ and *Mybl2*$^{\Delta/\Delta}$ ESCs with CPT and used Western blotting to directly monitor the activation of ATM using a phospho-specific antibody to S1987; a validated marker of ATM autoactivation. Strikingly *Mybl2*$^{\Delta/\Delta}$ ESCs were unable to efficiently activate ATM following the induction of DNA damage as compared to the *Mybl2*$^{+/+}$ ESCs (Figure 4F). This observation serves to strength the notion that MYBL2 is stem cell-specific activator of the ATM-dependent replication stress response.

To verify our findings suggesting a role for ATM in regulating the replication stress response in ESCs without using small molecule inhibitors, we generated *Atm*$^{-/-}$ ESCs and used DNA fibre analysis to monitor replication stress. Interestingly, this analysis demonstrated that genetic loss of ATM gave rise to a similar reduction in replication fork speed to that which we had previously observed in the *Mybl2*$^{+/+}$ ESCs treated with an ATM inhibitor (Figure 4G). Importantly, this reduced replication speed was not further reduced by treating the *Atm*$^{-/-}$ ESC with an ATM inhibitor, demonstrating that the replication stress phenotype induced by the ATM inhibitor did not arise due to off-target effects (Figure 4G). To investigate the role of ATM in suppressing replication stress further, we sought to determine whether loss of ATM activity could also lead to deregulation of replication factories. The number of replication factories in early S-phase was scored using imaris program after cells were subjected to a short pulse of IdU. As previously reported, *Mybl2*$^{\Delta/\Delta}$ ESCs displayed an increase in the number of replication factories when compared to *Mybl2*$^{+/+}$ ESCs (Figure 4H and EV4D). Consistent with our previous observations, both *Mybl2*$^{+/+}$ ESCs treated with ATM inhibitor, as well as *Atm*$^{-/-}$ ESCs also displayed an increase in number of replication factories (Figure 4H). Altogether, these data suggest that pluripotent stem cells rely on both the ATR and ATM kinases for proper replication progression in unperturbed conditions and that MYBL2 is a key component of the ATM replication stress response pathway in ESCs.

Whilst our data is consistent with a role for ATM in regulating replication in ESCs, since we have only used murine ESCs in our study, we felt that it was imperative to demonstrate that a similar phenomenon was also observed in other pluripotent stem cells but not in somatic cells. To investigate this, we carried out DNA fibre analysis on human induced pluripotent stem cells (iPSC) and primary/immortalised mouse embryonic fibroblasts (MEFs) in the presence or absence of an ATM or ATR inhibitor. Consistent with our findings using murine ESCs, both the ATM and ATR inhibitors induced a significant reduction in replication fork speed in the human iPSCs (Figure 4I and Appendix Figure S4A). However interestingly, the ATM inhibitor did not result in a significant reduction in fork speed in the primary and immortal MEFs (Figure 4I and Appendix Figure S4A). Moreover, similar to what we had observed in ESCs, exposure of iPSCs to the ATM inhibitor also increased the formation of UFBs (Appendix Figure S4B). These data confirm that ATM plays a role in suppressing replication stress in embryonic stem cells but not somatic cells.

The replication stress phenotype in *Mybl2*$^{\Delta/\Delta}$ ESCs is epistatic with loss of Mre11 nuclease activity

The MRN complex (MRE11-Rad50-NBS1) is a multi-functional protein complex involved in DNA repair, DNA replication and cell cycle checkpoint activation in part through its ability to

sense DNA damage and activate the ATM/ATR-dependent DNA damage response. Previously it has been shown that MYBL2 interacts with the MRN complex albeit the functional significance of this remains unclear (Henrich et al., 2017). Given functional links between the MRN complex, ATM and MYBL2, we sought to investigate whether the nucleolytic activity of MRE11, which is essential for its role in regulating DNA repair, plays a role in the MYBL2-ATM-dependent replication stress response pathway in ESCs. To test this, mirin, an inhibitor of the 3' to 5' exonuclease activity of MRE11 (Dupre et al., 2008) was utilised. *Mybl2*$^{+/+}$ and *Mybl2*$^{\Delta/\Delta}$ ESCs were treated with mirin before treatment with IdU and CldU to label nascent DNA synthesis (Figure 5A). DNA fibre analysis was performed and the effect of mirin on replication fork rates was determined. In *Mybl2*$^{+/+}$ ESCs, there was a substantial decrease in replication fork rate (Figure 5B), an increase in new origin firing (Figure 5D and 5E) and elevated replication fork instability in response to mirin treatment (Figure 5D and 5F). In contrast, mirin treatment had very little impact on replication fork rates, new origin firing and replication fork stability in the *Mybl2*$^{\Delta/\Delta}$ ESCs (Figure 5C,and 5D-F). These data suggests that both MYBL2 and the MRN complex are required for activation of the ATM-dependent replication stress response in ESCs.

Origin firing is deregulated in *Mybl2*$^{\Delta/\Delta}$ ESCs and ATMi-treated *Mybl2*$^{+/+}$ ESCs

It is known that the DDR pathway primarily controls replication in response to DNA damage by regulating origin firing via modulation of CDK and CDC7 kinase activity (Costanzo et al., 2003; Patil et al., 2013; Syljuasen et al., 2005; Zeman and Cimprich, 2014). Deregulation of CDK activity has been demonstrated to be a major cause of replication stress partly due to aberrant origin firing (Anda et al., 2016; Beck et al., 2012; Petermann et al., 2010; Sorensen and Syljuasen, 2012). Since ATM/ATR-mediated inhibition of CDK1 is reduced in *Mybl2*$^{\Delta/\Delta}$ ESCs (Figure 2), we initially sought to determine whether inhibition of CDK1 or a combination of CDK2 and CDK1 could rescue the replication defect observed in *Mybl2*$^{\Delta/\Delta}$ ESCs and wild type ESC after suppression of ATM kinase activity. To investigate this, both the *Mybl2*$^{+/+}$ and *Mybl2*$^{\Delta/\Delta}$ ESCs were treated with a CDK1 inhibitor (RO3306) before labelling of active replication and DNA fibre spreading (Figure EV5A). Analysis of replication structures revealed a very mild rescue of the elevated origin firing observed in *Mybl2*$^{\Delta/\Delta}$ ESCs treated with CDK1 inhbitor and in *Mybl2*$^{+/+}$ ESCs after treatment with both CDK1 inhibitor and ATM inhibitor, although, these differences were not staticitally significant (Figure EV5B). Moreover, inhibition of CDK1 in the *Mybl2*$^{\Delta/\Delta}$ ESCs partially normalized the replication fork speed to similar levels seen in the *Mybl2*$^{+/+}$ ESCs after CDK1 inhibition (Figure EV5C). Lastly, inhibition of CDK1 in ATM inhibited ESCs also resulted in a similar partial rescue of the replication progression defect (Figure EV5C). Based on this, we reasoned that a lack inhibition of origin firing following exposure to a CDK1 inhibitor could be

due to a compensatory effect of CDK2, thus we sought to suppress origin firing by inhibiting both CDK kinases (CDK1 and CDK2) by using the CDK1/2 inhibitor III (Higgs et al., 2015) (Figure EV5D). Similar to the CDK1i, the CDK1/2 inhibitor also did not dramatically reduce origin firing in *Mybl2*$^{+/+}$ ESCs (neither at 3uM nor at 25uM) but did result in a reduced rate of replication (Figure EV5E, EV5F and EV5G). In contrast, CDK1/2 inhibition in *Mybl2*$^{\Delta/\Delta}$ ESCs and wild type ESCs treated with an ATMi lead to a reduction in origin firing and a partial rescue of fork speed (Figure EV5E and EV5F). From these observations, it would indicate that neither CDK1 nor CDK2 play a major role in regulating new origin firing in WT ESCs and the mild recovery of replication rates in *Mybl2*$^{\Delta/\Delta}$ ESCs following CDK1/2 inhibition may arise as a consequence of the slightly better suppression of new origin firing in these cells.

In view of these results, we hypothesized that deregulation of CDC7 may underlie the increased new origin firing and reduced replication rates exhibited by *Mybl2*$^{\Delta/\Delta}$ ESCs (Figure 6A) (Jackson et al., 1993; Yeeles et al., 2015). To investigate this, *Mybl2*$^{+/+}$ and *Mybl2*$^{\Delta/\Delta}$ ESCs were treated with the CDC7 inhibitor PHA-767491 (10uM) before labelling active replication forks (Figure 6B). Consistent with this hypothesis, treatment of the *Mybl2*$^{+/+}$ ESCs with a CDC7 inhibitor resulted in a significant decrease in new origin firing (Figure 6C). Moreover, the elevated origin firing observed in the *Mybl2*$^{\Delta/\Delta}$ ESCs as well as in the *Mybl2*$^{+/+}$ ESCs treated with ATM inhibitor was significantly decreased to levels comparable to the *Mybl2*$^{+/+}$ ESC (Figure 6C). Interestingly, whilst CDC7 inhibition had very little impact on replication rates in *Mybl2*$^{+/+}$ ESCs, remarkably, this resulted in a complete rescue of replication fork speed in *Mybl2*$^{\Delta/\Delta}$ ESCs or WT ESCs treated with an inhibitor (Figure 6D). Consistent with this observation, inhibition of CDC7 completely rescued replication fork stability in ESCs lacking Mybl2 or ATM activity (Figure 6E). Importantly, our data indicated that the CDC7-dependent increase in origin firing was not due to an increase of CDC7 protein levels (Figure 6F). Together these data indicate that the elevated levels of replication stress resulting from a loss of MYBL2 or ATM activity is caused by aberrant CDC7-dependent firing of replication forks and that a replication stress response pathway regulated by MYBL2 and ATM function to modulate CDC7 activity to maintain genomic integrity (Figure 7).

Discussion

ESCs possess unique cellular properties that are tailored to their vital roles for successful development of the mammalian embryo**.** Their capacity to differentiate into a diverse array of functionally distinct cell types means that the acquisition of detrimental mutations early in this process could have catastrophic consequences for the whole embryo (Blanpain et al., 2011). Under these circumstances, tight regulation of replication progression is paramount to

maintain genomic integrity in these cells. ATR has been shown to be the principal replication stress responsive kinase required to maintain fork stability (Cimprich and Cortez, 2008; Paulsen and Cimprich, 2007) and suppress the initiation of replication in the presence of damaged DNA (Costanzo et al., 2003; Patil et al., 2013; Syljuasen et al., 2005; Zeman and Cimprich, 2014). Consistent with this role, our work shows that the inhibition of ATR in both pluripotent stem cells (mouse ESCs and human iPSCs) as well as in primary and immortal somatic cells (MEFs) leads to a slow down in replication fork progression.

Importantly however, our data also demonstrates a role for ATM, which is normally activated exclusively in response to DSBs (Bakkenist and Kastan, 2003; Lee and Paull, 2004; Shiloh, 2003), in regulating the replication stress response in ESCs, in part by facilitating the activation of CHK1. Whilst the mechanisms with which ATM regulates replication in ESCs have not been defined, it is clear that it does not function to suppress new origin firing and regulate elongation through the conventional CHK1-CDC25A-CDK2 DNA damage checkpoint pathway that has been identified in somatic cells (Falck et al., 2001). Rather, our data would indicate that CDC7 plays a more pivotal role in regulating replication origin firing than CDKs in ESCs but whether ATM directly or indirectly regulates CDC7 activation remains to be determined. Despite this, our work raises several interesting questions: Why is ATM required to regulate the replication stress response in ESCs and how does its activation in ESCs differ from that in somatic cells? It has been recently demonstrated that ESCs are very tolerant of high levels of replicative stress caused by a failure to complete replication in a single cell cycle. It has been suggested that the increased propensity for replication forks in ESCs to undergo reversal coupled with their high reliance on replication coupled-repair mechanisms to deal with the under-replicated DNA allows these cells to prevent fork collapse and chromosomal breakage in the face of high levels of replication stress. Based on this, it is likely that many critical regulators of DNA replication and the replication stress response will be limiting and as a consequence, factors such as ATR require aid from back up pathways, such as those regulated by ATM. Conversely, whilst ESCs actively induce replication fork reversal to maintain genome stability from the multiple rounds of discontinuous replication, it is evident that this process is not infalable and as such, DSBs do result from replication fork collapse. Therefore, it is conceivable that this is why ESCs are more reliant on ATM to respond to DNA damage arising in S-phase than somatic cells.

In relation to whether the activation of ATM in response to replication differs in ESCs from that in somatic cells, given that DSBs are generated as a result of the unusual process of replication in ESCs and that we have observed that MRN complex is required to suppress

replication stress, this would be consistent with the MRN complex sensing DSBs and then activating ATM. However, it is known that ESCs have a more relaxed chromatin state and that the strength of DDR activation in these cells is dependent on the level of chromatin compaction. Given that it has been previously shown that ATM can be activated in the absence of DSBs by alterating chromatin accessibility (Bakkenist et al., 2003), it is possible that the increased chromatin accessibility in ESCs allows ATM to respond to a wider spectrum of DNA lesions or structures than it usually would in somatic cells where regions of eu- and heterochromatin are more clearly defined. In addition to this, we have demonstrated that the activation of the MRN-ATM-dependent replication stress response in ESCs also requires MYBL2. Whilst it is not clear why MYBL2 is required to activate the ATM-dependent replication stress response, it has been previously shown that MYBL2 binds to the MRN complex and is recruited to sites of DNA damage. However, it was suggested that MYBL2 does not play a role in regulating DNA repair and this interaction was associated with activation of the DNA damage G2/M checkpoint through its ability to act as a transcription factor. In keeping with this report, we observed that *Mybl2*$^{\Delta/\Delta}$ ESCs failed to properly activate the DNA damage-induced G2/M checkpoint but whether this resulted from a reduction in the expression of genes involved in the G2-M transition or a failure to properly activate CHK1 remains to be determined. Nevertheless, our RNA-seq data from *Mybl2*$^{\Delta/\Delta}$ ESCs did not identify any significant alterations in genes associated with DNA replication (data not shown) suggesting that in ESCs MYBL2 maybe also be functioning as a component of the replication stress response independent of its role as a transcription factor.

Whilst our work clearly demonstrates that MYBL2, in conjunction with ATM, is important for suppressing replication stress in ESCs, it is currently not clear as to what the underlying cause is. Ahuja et al. (2016) reported that the endogenous high level of replication stress present in ESCs does not arise as a consequence of high levels of oxidative damage, deoxynucleotide (dNTP) depletion or increased transcription-replication collisions but was rather due to the very short G1 phase preventing sufficient time for replication stress resolution. However, from our observations, it is clear that the loss of MYBL2 or ATM significantly increases the levels of endogenous cellular replication stress in ESCs without affecting the length of G1 phase. Interestingly, we demonstrated that the high levels of replication stress exhibited by ESCs lacking MYBL2 or ATM could be rescued by a short incubation with a CDC7 inhibitor. Although it was suggested by Ahuja et al. (2016) that the rescue of endogenous replication stress in ESCs following inhibition of CDC7 was solely due to a lengthening of G1 phase, this was achieved after ESCs were released from a transient G1 arrest imposed by an 8 h incubation with the CDC7 inhibitor (PHA-767491). In contrast, we could observe a rescue of replication rates in MYBL2 or ATM deficient ESCs after a 1.5 h

514 incubation with the same CDC7 inhibitor and at the same concentration, which is unlikely to
515 significantly affect the duration of G1 phase.
516
517 Taken together, our work identifies ATM as a critical regulator of the replication stress
518 response pathway in ESCs and demonstrate that MYBL2 functions to suppress replication
519 stress, in part through its ability to activate ATM. Furthermore, we believe these findings are
520 likely to have clinical rammifications since aberrant regulation of MYBL2 may affect the
521 sensitivity of tumour cells to inhibitors of the ATM-dependent DNA damage response.
522
523 **Acknowledgements:** The authors wish to thank the members of the Garcia lab for advice
524 and constructive criticisms. Dr Ruth Densham, Dr Clare Davies and Dr Martin Higgs for
525 advice and critical reading of the manuscript; Dr Sovan Sarkar for the immortal MEFs and
526 Professor Tatjana Stankovic for the *Atm*$^{+/-}$ mice. The authors also wish to thank the animal
527 facility and cell sorter facility at the University of Birmingham. G.S.S is funded by a CR-UK
528 Programme Grant (C17183/A23303). This work was also funded by a MRC PhD studenthip
529 to D.B and an ISSF Wellcome Trust critical data award (1000599) to P.G.
530
531 **Author contributions**
532 D.B conceived and performed experiments, acquired and analyzed data, and wrote the
533 manuscript. N.V, R.A, E.G, C.W and M.M performed experiments, acquired and analyzed
534 data. G.J.M provided reagents. E.P and A.G helped with experimental design, interpretation
535 and critical discussion of the data. G.S.S performed experiments, helped with experimental
536 design, interpretation and critical discussion of the data and wrote the manuscript. P.G
537 conceived and performed experiments, acquired and analyzed data, wrote the manuscript
538 and managed the project.
539
540 **Declaration of interest:**
541 The authors declare no potential conflict of interest.
542
543 **References**

544 Aguilera, A., and Gomez-Gonzalez, B. (2008). Genome instability: a mechanistic view of its causes
545 and consequences. Nat Rev Genet *9*, 204-217.
546 Ahuja, A.K., Jodkowska, K., Teloni, F., Bizard, A.H., Zellweger, R., Herrador, R., Ortega, S., Hickson,
547 I.D., Altmeyer, M., Mendez, J., *et al.* (2016). A short G1 phase imposes constitutive replication stress
548 and fork remodelling in mouse embryonic stem cells. Nat Commun *7*, 10660.
549 Anda, S., Rothe, C., Boye, E., and Grallert, B. (2016). Consequences of abnormal CDK activity in S
550 phase. Cell Cycle *15*, 963-973.
551 Bakkenist, C.J., and Kastan, M.B. (2003). DNA damage activates ATM through intermolecular
552 autophosphorylation and dimer dissociation. Nature *421*, 499-506.

553 Ballabeni, A., Park, I.H., Zhao, R., Wang, W., Lerou, P.H., Daley, G.Q., and Kirschner, M.W. (2011). Cell
554 cycle adaptations of embryonic stem cells. Proc Natl Acad Sci U S A *108*, 19252-19257.
555 Bartek, J., Lukas, C., and Lukas, J. (2004). Checking on DNA damage in S phase. Nat Rev Mol Cell Biol
556 *5*, 792-804.
557 Baumann, C., Korner, R., Hofmann, K., and Nigg, E.A. (2007). PICH, a centromere-associated SNF2
558 family ATPase, is regulated by Plk1 and required for the spindle checkpoint. Cell *128*, 101-114.
559 Bayley, R., Blakemore, D., Cancian, L., Dumon, S., Volpe, G., Ward, C., Almaghrabi, R., Gujar, J.,
560 Reeve, N., Raghavan, M.*, et al.* (2018). MYBL2 Supports DNA Double Strand Break Repair in
561 Hematopoietic Stem Cells. Cancer Res *78*, 5767-5779.
562 Beck, H., Nahse-Kumpf, V., Larsen, M.S., O'Hanlon, K.A., Patzke, S., Holmberg, C., Mejlvang, J., Groth,
563 A., Nielsen, O., Syljuasen, R.G.*, et al.* (2012). Cyclin-dependent kinase suppression by WEE1 kinase
564 protects the genome through control of replication initiation and nucleotide consumption. Mol Cell
565 Biol *32*, 4226-4236.
566 Bencokova, Z., Kaufmann, M.R., Pires, I.M., Lecane, P.S., Giaccia, A.J., and Hammond, E.M. (2009).
567 ATM activation and signaling under hypoxic conditions. Mol Cell Biol *29*, 526-537.
568 Blanpain, C., Mohrin, M., Sotiropoulou, P.A., and Passegue, E. (2011). DNA-damage response in
569 tissue-specific and cancer stem cells. Cell Stem Cell *8*, 16-29.
570 Broderick, R., Nieminuszczy, J., Blackford, A.N., Winczura, A., and Niedzwiedz, W. (2015). TOPBP1
571 recruits TOP2A to ultra-fine anaphase bridges to aid in their resolution. Nat Commun *6*, 6572.
572 Cam, H., Easton, J.B., High, A., and Houghton, P.J. (2010). mTORC1 signaling under hypoxic
573 conditions is controlled by ATM-dependent phosphorylation of HIF-1alpha. Mol Cell *40*, 509-520.
574 Cervantes, R.B., Stringer, J.R., Shao, C., Tischfield, J.A., and Stambrook, P.J. (2002). Embryonic stem
575 cells and somatic cells differ in mutation frequency and type. Proc Natl Acad Sci U S A *99*, 3586-3590.
576 Chan, K.L., and Hickson, I.D. (2011). New insights into the formation and resolution of ultra-fine
577 anaphase bridges. Semin Cell Dev Biol *22*, 906-912.
578 Chan, Y.W., Fugger, K., and West, S.C. (2018). Unresolved recombination intermediates lead to ultra-
579 fine anaphase bridges, chromosome breaks and aberrations. Nat Cell Biol *20*, 92-103.
580 Cimprich, K.A., and Cortez, D. (2008). ATR: an essential regulator of genome integrity. Nat Rev Mol
581 Cell Biol *9*, 616-627.
582 Coronado, D., Godet, M., Bourillot, P.Y., Tapponnier, Y., Bernat, A., Petit, M., Afanassieff, M.,
583 Markossian, S., Malashicheva, A., Iacone, R.*, et al.* (2013). A short G1 phase is an intrinsic
584 determinant of naive embryonic stem cell pluripotency. Stem Cell Res *10*, 118-131.
585 Costanzo, V., Shechter, D., Lupardus, P.J., Cimprich, K.A., Gottesman, M., and Gautier, J. (2003). An
586 ATR- and Cdc7-dependent DNA damage checkpoint that inhibits initiation of DNA replication. Mol
587 Cell *11*, 203-213.
588 de Klein, A., Muijtjens, M., van Os, R., Verhoeven, Y., Smit, B., Carr, A.M., Lehmann, A.R., and
589 Hoeijmakers, J.H. (2000). Targeted disruption of the cell-cycle checkpoint gene ATR leads to early
590 embryonic lethality in mice. Curr Biol *10*, 479-482.
591 Dimitrova, D.S., and Berezney, R. (2002). The spatio-temporal organization of DNA replication sites is
592 identical in primary, immortalized and transformed mammalian cells. J Cell Sci *115*, 4037-4051.
593 Down, C.F., Millour, J., Lam, E.W., and Watson, R.J. (2012). Binding of FoxM1 to G2/M gene
594 promoters is dependent upon B-Myb. Biochim Biophys Acta *1819*, 855-862.
595 Dupre, A., Boyer-Chatenet, L., Sattler, R.M., Modi, A.P., Lee, J.H., Nicolette, M.L., Kopelovich, L.,
596 Jasin, M., Baer, R., Paull, T.T.*, et al.* (2008). A forward chemical genetic screen reveals an inhibitor of
597 the Mre11-Rad50-Nbs1 complex. Nat Chem Biol *4*, 119-125.
598 Ewald, B., Sampath, D., and Plunkett, W. (2008). ATM and the Mre11-Rad50-Nbs1 complex respond
599 to nucleoside analogue-induced stalled replication forks and contribute to drug resistance. Cancer
600 Res *68*, 7947-7955.
601 Falck, J., Mailand, N., Syljuasen, R.G., Bartek, J., and Lukas, J. (2001). The ATM-Chk2-Cdc25A
602 checkpoint pathway guards against radioresistant DNA synthesis. Nature *410*, 842-847.
603 Ferreira, J., and Carmo-Fonseca, M. (1997). Genome replication in early mouse embryos follows a
604 defined temporal and spatial order. J Cell Sci *110 (Pt 7)*, 889-897.

Fujii-Yamamoto, H., Kim, J.M., Arai, K., and Masai, H. (2005). Cell cycle and developmental regulations of replication factors in mouse embryonic stem cells. J Biol Chem *280*, 12976-12987.

Garcia, P., Berlanga, O., Watson, R., and Frampton, J. (2005). Generation of a conditional allele of the B-myb gene. Genesis *43*, 189-195.

Ge, X.Q., and Blow, J.J. (2010). Chk1 inhibits replication factory activation but allows dormant origin firing in existing factories. J Cell Biol *191*, 1285-1297.

Guo, Z., Kumagai, A., Wang, S.X., and Dunphy, W.G. (2000). Requirement for Atr in phosphorylation of Chk1 and cell cycle regulation in response to DNA replication blocks and UV-damaged DNA in Xenopus egg extracts. Genes Dev *14*, 2745-2756.

Heald, R., McLoughlin, M., and McKeon, F. (1993). Human wee1 maintains mitotic timing by protecting the nucleus from cytoplasmically activated Cdc2 kinase. Cell *74*, 463-474.

Hengeveld, R.C., de Boer, H.R., Schoonen, P.M., de Vries, E.G., Lens, S.M., and van Vugt, M.A. (2015). Rif1 Is Required for Resolution of Ultrafine DNA Bridges in Anaphase to Ensure Genomic Stability. Dev Cell *34*, 466-474.

Henrich, S.M., Usadel, C., Werwein, E., Burdova, K., Janscak, P., Ferrari, S., Hess, D., and Klempnauer, K.H. (2017). Interplay with the Mre11-Rad50-Nbs1 complex and phosphorylation by GSK3beta implicate human B-Myb in DNA-damage signaling. Sci Rep *7*, 41663.

Higgs, M.R., Reynolds, J.J., Winczura, A., Blackford, A.N., Borel, V., Miller, E.S., Zlatanou, A., Nieminuszczy, J., Ryan, E.L., Davies, N.J., *et al.* (2015). BOD1L Is Required to Suppress Deleterious Resection of Stressed Replication Forks. Mol Cell *59*, 462-477.

Iwahori, S., Kohmon, D., Kobayashi, J., Tani, Y., Yugawa, T., Komatsu, K., Kiyono, T., Sugimoto, N., and Fujita, M. (2014). ATM regulates Cdt1 stability during the unperturbed S phase to prevent re-replication. Cell Cycle *13*, 471-481.

Jackson, A.L., Pahl, P.M., Harrison, K., Rosamond, J., and Sclafani, R.A. (1993). Cell cycle regulation of the yeast Cdc7 protein kinase by association with the Dbf4 protein. Mol Cell Biol *13*, 2899-2908.

Kapinas, K., Grandy, R., Ghule, P., Medina, R., Becker, K., Pardee, A., Zaidi, S.K., Lian, J., Stein, J., van Wijnen, A., *et al.* (2013). The abbreviated pluripotent cell cycle. J Cell Physiol *228*, 9-20.

Katzen, A.L., Jackson, J., Harmon, B.P., Fung, S.M., Ramsay, G., and Bishop, J.M. (1998). Drosophila myb is required for the G2/M transition and maintenance of diploidy. Genes Dev *12*, 831-843.

Khanna, K.K., Lavin, M.F., Jackson, S.P., and Mulhern, T.D. (2001). ATM, a central controller of cellular responses to DNA damage. Cell Death Differ *8*, 1052-1065.

Knight, A.S., Notaridou, M., and Watson, R.J. (2009). A Lin-9 complex is recruited by B-Myb to activate transcription of G2/M genes in undifferentiated embryonal carcinoma cells. Oncogene *28*, 1737-1747.

Lee, J.H., and Paull, T.T. (2004). Direct activation of the ATM protein kinase by the Mre11/Rad50/Nbs1 complex. Science *304*, 93-96.

Lefebvre, C., Rajbhandari, P., Alvarez, M.J., Bandaru, P., Lim, W.K., Sato, M., Wang, K., Sumazin, P., Kustagi, M., Bisikirska, B.C., *et al.* (2010). A human B-cell interactome identifies MYB and FOXM1 as master regulators of proliferation in germinal centers. Mol Syst Biol *6*, 377.

Li, D.W., Yang, Q., Chen, J.T., Zhou, H., Liu, R.M., and Huang, X.T. (2005). Dynamic distribution of Ser-10 phosphorylated histone H3 in cytoplasm of MCF-7 and CHO cells during mitosis. Cell Res *15*, 120-126.

Liu, Q., Guntuku, S., Cui, X.S., Matsuoka, S., Cortez, D., Tamai, K., Luo, G., Carattini-Rivera, S., DeMayo, F., Bradley, A., *et al.* (2000). Chk1 is an essential kinase that is regulated by Atr and required for the G(2)/M DNA damage checkpoint. Genes Dev *14*, 1448-1459.

Lorvellec, M., Dumon, S., Maya-Mendoza, A., Jackson, D., Frampton, J., and Garcia, P. (2010). B-Myb is critical for proper DNA duplication during an unperturbed S phase in mouse embryonic stem cells. Stem Cells *28*, 1751-1759.

Luciani, M.G., Oehlmann, M., and Blow, J.J. (2004). Characterization of a novel ATR-dependent, Chk1-independent, intra-S-phase checkpoint that suppresses initiation of replication in Xenopus. J Cell Sci *117*, 6019-6030.

Marheineke, K., and Hyrien, O. (2004). Control of replication origin density and firing time in Xenopus egg extracts: role of a caffeine-sensitive, ATR-dependent checkpoint. J Biol Chem *279*, 28071-28081.

Martinez, I., and Dimaio, D. (2011). B-Myb, cancer, senescence, and microRNAs. Cancer Res *71*, 5370-5373.

Maya-Mendoza, A., Moudry, P., Merchut-Maya, J.M., Lee, M., Strauss, R., and Bartek, J. (2018). High speed of fork progression induces DNA replication stress and genomic instability. Nature *559*, 279-284.

Moiseeva, T.N., Yin, Y., Calderon, M.J., Qian, C., Schamus-Haynes, S., Sugitani, N., Osmanbeyoglu, H.U., Rothenberg, E., Watkins, S.C., and Bakkenist, C.J. (2019). An ATR and CHK1 kinase signaling mechanism that limits origin firing during unperturbed DNA replication. Proc Natl Acad Sci U S A *116*, 13374-13383.

Murga, M., Jaco, I., Fan, Y., Soria, R., Martinez-Pastor, B., Cuadrado, M., Yang, S.M., Blasco, M.A., Skoultchi, A.I., and Fernandez-Capetillo, O. (2007). Global chromatin compaction limits the strength of the DNA damage response. J Cell Biol *178*, 1101-1108.

Olcina, M., Lecane, P.S., and Hammond, E.M. (2010). Targeting hypoxic cells through the DNA damage response. Clin Cancer Res *16*, 5624-5629.

Olcina, M.M., Foskolou, I.P., Anbalagan, S., Senra, J.M., Pires, I.M., Jiang, Y., Ryan, A.J., and Hammond, E.M. (2013). Replication stress and chromatin context link ATM activation to a role in DNA replication. Mol Cell *52*, 758-766.

Osterloh, L., von Eyss, B., Schmit, F., Rein, L., Hubner, D., Samans, B., Hauser, S., and Gaubatz, S. (2007). The human synMuv-like protein LIN-9 is required for transcription of G2/M genes and for entry into mitosis. EMBO J *26*, 144-157.

Ostling, O., and Johanson, K.J. (1984). Microelectrophoretic study of radiation-induced DNA damages in individual mammalian cells. Biochem Biophys Res Commun *123*, 291-298.

Patil, M., Pabla, N., and Dong, Z. (2013). Checkpoint kinase 1 in DNA damage response and cell cycle regulation. Cell Mol Life Sci *70*, 4009-4021.

Pattschull, G., Walz, S., Grundl, M., Schwab, M., Ruhl, E., Baluapuri, A., Cindric-Vranesic, A., Kneitz, S., Wolf, E., Ade, C.P., *et al.* (2019). The Myb-MuvB Complex Is Required for YAP-Dependent Transcription of Mitotic Genes. Cell Rep *27*, 3533-3546 e3537.

Paulsen, R.D., and Cimprich, K.A. (2007). The ATR pathway: fine-tuning the fork. DNA Repair (Amst) *6*, 953-966.

Petermann, E., Woodcock, M., and Helleday, T. (2010). Chk1 promotes replication fork progression by controlling replication initiation. Proc Natl Acad Sci U S A *107*, 16090-16095.

Rodriguez-Acebes, S., Mouron, S., and Mendez, J. (2018). Uncoupling fork speed and origin activity to identify the primary cause of replicative stress phenotypes. J Biol Chem *293*, 12855-12861.

Sadasivam, S., and DeCaprio, J.A. (2013). The DREAM complex: master coordinator of cell cycle-dependent gene expression. Nat Rev Cancer *13*, 585-595.

Sadasivam, S., Duan, S., and DeCaprio, J.A. (2012). The MuvB complex sequentially recruits B-Myb and FoxM1 to promote mitotic gene expression. Genes Dev *26*, 474-489.

Saldivar, J.C., Hamperl, S., Bocek, M.J., Chung, M., Bass, T.E., Cisneros-Soberanis, F., Samejima, K., Xie, L., Paulson, J.R., Earnshaw, W.C., *et al.* (2018). An intrinsic S/G2 checkpoint enforced by ATR. Science *361*, 806-810.

Savatier, P., Huang, S., Szekely, L., Wiman, K.G., and Samarut, J. (1994). Contrasting patterns of retinoblastoma protein expression in mouse embryonic stem cells and embryonic fibroblasts. Oncogene *9*, 809-818.

Shechter, D., Costanzo, V., and Gautier, J. (2004). ATR and ATM regulate the timing of DNA replication origin firing. Nat Cell Biol *6*, 648-655.

Shiloh, Y. (2003). ATM and related protein kinases: safeguarding genome integrity. Nat Rev Cancer *3*, 155-168.

Singh, N.P., McCoy, M.T., Tice, R.R., and Schneider, E.L. (1988). A simple technique for quantitation of low levels of DNA damage in individual cells. Exp Cell Res *175*, 184-191.

Sitzmann, J., Noben-Trauth, K., Kamano, H., and Klempnauer, K.H. (1996). Expression of B-Myb during mouse embryogenesis. Oncogene *12*, 1889-1894.

Sorensen, C.S., and Syljuasen, R.G. (2012). Safeguarding genome integrity: the checkpoint kinases ATR, CHK1 and WEE1 restrain CDK activity during normal DNA replication. Nucleic Acids Res *40*, 477-486.

Syljuasen, R.G., Sorensen, C.S., Hansen, L.T., Fugger, K., Lundin, C., Johansson, F., Helleday, T., Sehested, M., Lukas, J., and Bartek, J. (2005). Inhibition of human Chk1 causes increased initiation of DNA replication, phosphorylation of ATR targets, and DNA breakage. Mol Cell Biol *25*, 3553-3562.

Tanaka, Y., Patestos, N.P., Maekawa, T., and Ishii, S. (1999). B-myb is required for inner cell mass formation at an early stage of development. J Biol Chem *274*, 28067-28070.

Tarasov, K.V., Tarasova, Y.S., Tam, W.L., Riordon, D.R., Elliott, S.T., Kania, G., Li, J., Yamanaka, S., Crider, D.G., Testa, G.*, et al.* (2008). B-MYB is essential for normal cell cycle progression and chromosomal stability of embryonic stem cells. PLoS One *3*, e2478.

Valerie, K., and Povirk, L.F. (2003). Regulation and mechanisms of mammalian double-strand break repair. Oncogene *22*, 5792-5812.

Ward, C., Volpe, G., Cauchy, P., Ptasinska, A., Almaghrabi, R., Blakemore, D., Nafria, M., Kestner, D., Frampton, J., Murphy, G.*, et al.* (2018). Fine-Tuning Mybl2 Is Required for Proper Mesenchymal-to-Epithelial Transition during Somatic Reprogramming. Cell Rep *24*, 1496-1511 e1498.

Watanabe, N., Broome, M., and Hunter, T. (1995). Regulation of the human WEE1Hu CDK tyrosine 15-kinase during the cell cycle. EMBO J *14*, 1878-1891.

Wolter, P., Hanselmann, S., Pattschull, G., Schruf, E., and Gaubatz, S. (2017). Central spindle proteins and mitotic kinesins are direct transcriptional targets of MuvB, B-MYB and FOXM1 in breast cancer cell lines and are potential targets for therapy. Oncotarget *8*, 11160-11172.

Yeeles, J.T., Deegan, T.D., Janska, A., Early, A., and Diffley, J.F. (2015). Regulated eukaryotic DNA replication origin firing with purified proteins. Nature *519*, 431-435.

Zeman, M.K., and Cimprich, K.A. (2014). Causes and consequences of replication stress. Nat Cell Biol *16*, 2-9.

Zhao, B., Zhang, W.D., Duan, Y.L., Lu, Y.Q., Cun, Y.X., Li, C.H., Guo, K., Nie, W.H., Li, L., Zhang, R.*, et al.* (2015). Filia Is an ESC-Specific Regulator of DNA Damage Response and Safeguards Genomic Stability. Cell Stem Cell *16*, 684-698.

Figure legends

Figure 1. *Mybl2*$^{\Delta/\Delta}$ ESCs display fork instability and a replication stress phenotype leading to unreplicated DNA, Increase replication-associated DSB and genome instability

A) Distribution curve of replication fork rates for *Mybl2*$^{+/+}$ and *Mybl2*$^{\Delta/\Delta}$ ESCs. Statistical analysis was performed using the Mann Whitney U test. n=6 experimental replicates. A minimum of 490 replication forks were counted.(**** p< 0.0001).

B) Left panel: representative elongating replication forks (stable and unstable). Quantification of the average IdU/CldU ratio in the *Mybl2*$^{+/+}$ and *Mybl2*$^{\Delta/\Delta}$ ESCs. Percentage of highly unstable forks (ratio above 2) are indicated. Y-axis was cut to change scale and display large values. Statistical analysis was performed using the Mann Whitney U test. (**** p< 0.0001).

At least 450 ratios were recorded from 6 experimental replicates.

C) The length of both CldU labels surrounding IdU tracks (newly fired origins) was measured before calculating a ratio representing symmetry around new origins. Quantification of the average positive ratio in the *Mybl2*$^{+/+}$ and *Mybl2*$^{\Delta/\Delta}$ ESCs. Y-axis was cut to change scale and display large values. Statistical analysis was performed using the Mann Whitney U test. 55 and 75 ratios were recorded in the *Mybl2*$^{+/+}$ and *Mybl2*$^{\Delta/\Delta}$ respectively from 3 replicates (**** p< 0.0001).

D) Representative image showing the presence of UFB by positive Immunostaining for PICH. (Scale bar 10µm). Frequency of anaphases positive for UFBs relative to all anaphases in the *Mybl2*$^{+/+}$ and *Mybl2*$^{\Delta/\Delta}$ ESCs. At least 75 anaphases were counted per experimental group from 3 independent experiments. Statistical analysis was performed using an unpaired two-tailed t-test (**** p< 0.0001).

E) Representative images for comets in *Mybl2*$^{+/+}$ and *Mybl2*$^{\Delta/\Delta}$ untreated and *Mybl2*$^{+/+}$ and *Mybl2*$^{\Delta/\Delta}$ plus CPT (20x magnification). (Scale bar 50µm).

F) Quantification of the mean and distributions of olive tail moments in Mybl2$^{+/+}$ and Mybl2$^{\Delta/\Delta}$ untreated and CPT-treated. Y-axis was cut to change scale and display large values. Statistical analysis using Mann Whitney U tests. At least 300 comets were measured for each group from 5 experimental replicates *(***** p< 0.0001).

G) Frequency of EdU positive cells with over 6 53BP1 foci in *Mybl2*$^{+/+}$, *Mybl2*$^{\Delta/\Delta}$ untreated and *Mybl2*$^{+/+}$ and *Mybl2*$^{\Delta/\Delta}$ plus CPT. Error bars represent SEM. Statistical analysis using unpaired two-tailed t-test. At least 200 EdU positive nuclei were analysed from 4 experimental repeats.

Figure 2. MYBL2-ablated ESCs fail to activate the DNA-damaged activated, G2/M checkpoint

A) Cells were treated for 1.5 hours with 5µM CPT, before sequential addition of IdU and CldU for 20 minutes each. Frequency of new firing origins (relative to total structures counted) from *Mybl2*$^{+/+}$ and *Mybl2*$^{\Delta/\Delta}$ ESCs treated or not with CPT (n=3 independent experiments; Error bars indicate SEM). Statistical analysis using two- tailed unpaired t-test.

(B) Distribution of replication rate in *Mybl2*$^{+/+}$ and *Mybl2*$^{\Delta/\Delta}$ ESC treated or not with CPT as above. Statistical analysis was carried out using unpaired Mann Whitney U tests. A minimum of 200 forks were quantified for each of the genotypes and conditions shown from 3 independent repeats (*p < 0.05; **p< 0.01; ***p< 0.001; **** p< 0.0001).

C) ESCs were treated with or without CPT for 4 hours before 0.1ug/ml colcemid was added during the final 3.5 hours of treatment. Representative image of H3-pS10 positive cells (turquoise). (Scale bar 10µm). Frequency of H3-pS10 positive cells in *Mybl2*$^{+/+}$ and *Mybl2*$^{\Delta/\Delta}$ ESCs. Data from three independent experiments. Error bars represent SEM. Statistical analysis was carried out using a two-tailed unpaired t-test (*p < 0.05; **p< 0.01; ns= no significant).

D) P-CDK1 (Tyr15), CDK1 and Beta-actin expression levels of *Mybl2*$^{+/+}$ and *Mybl2*$^{\Delta/\Delta}$ ESCs with or without CPT treatment analyzed by immunoblotting. Bar graph represents average band density of P-CDK1 in *Mybl2*$^{\Delta/\Delta}$ ESCs relative to loading control and relative to the MYBL2$^{+/+}$ from 6 repeats. Error bars represent SEM. Statistical analysis was carried out using a two-tailed unpaired t-test (**p< 0.01).

Figure 3. Proficient ATR dependent CHK1 activation in MYBL2- ablated ESC.

A) Immunoblot showing the levels of phosphorylated CHK1 (Ser345) and GAPDH in the *Mybl2*$^{+/+}$ and *Mybl2*$^{\Delta/\Delta}$ ESCs with or without CPT treatment (2.5µM CPT for 4 hours).

B) Immunoblot showing the levels of P-CHK1 (Ser345) and GADPH in irradiated *Mybl2*$^{+/+}$, *Mybl2*$^{+/\Delta}$ and *Mybl2*$^{\Delta/\Delta}$ ESCs with or without 3 hours inhibitor treatment: ATR (AZ20, 5µM) and ATM (Ku60019, 10µM). Cells were also exposed to 5Gy irradiation before the final hour of inhibitor treatment.. Bar graph (lower panel) represents average band density of P-CHK1 in *Mybl2*$^{\Delta/\Delta}$ ESCs relative to CHK1 and relative to untreated cells from at least two independent repeats. Error bars represent SEM. Statistical analysis was carried out using a two-tailed unpaired t-test (*p< 0.05).

C) Cells were treated for 1.5 hours with 5µM AZ20, before sequential addition of IdU and CldU for 20 minutes each. Dot plot representing the effect of ATR inhibition upon replication rate in *Mybl2*$^{+/+}$ and *Mybl2*$^{\Delta/\Delta}$ ESC. Statistical analysis of distributions was carried out using

unpaired Mann Whitney U tests. A minimum of 240 forks were quantified for each of the genotypes and conditions shown from 2 independent repeats (**** p< 0.0001)

D) Frequency of new firing origins (relative to total structures counted) from *Mybl2*$^{+/+}$ and *Mybl2*$^{\Delta/\Delta}$ ESCs treated or not with ATR inhibitor AZ20. At least 500 replication structures were counted per treatment from two independent repeats. Statistical analysis using two-tailed unpaired t-test.(*p< 0.05; ns= no significant).

E) Distribution and average of IdU/CldU fork ratio in *Mybl2*$^{+/+}$ and *Mybl2*$^{\Delta/\Delta}$ ESCs with or without ATR inhibitor treatment. Percentage of highly unstable forks (ratio above 2) are indicated. Dotted line at 1 indicates positive ratio. Y-axis was cut to change scale and display large values. Statistical analysis was carried out using the Mann Whitney U test. At least 150 ratios were calculated per treatment group from two independent repeats (*p < 0.05; **p< 0.01; ***p< 0.001; **** p< 0.0001).

Figure 4. ATM kinase and MYBL2 function to regulate replication in pluripotent stem cells.

A) Scheme of the protocol. ESCs were treated with 10µM KU60019 for 1.5 hours before sequential addition of IdU and CldU for 20 minutes each. DNA was treated and visualised as previously described.

B) Distribution of replication rate after treatment with/without ATM inhibitor. Statistical analysis of distributions was carried out using an unpaired Mann Whitney U test. n=4. A minimum of 270 forks was measured for each condition (**** p< 0.0001).

C) Distribution of the average IdU/CldU ratio in *Mybl2*$^{+/+}$ and *Mybl2*$^{\Delta/\Delta}$ ESCs with or without ATM inhibitor treatment. Percentage of highly unstable forks (ratio above 2) are indicated. Dotted line at 1 indicates positive ratio. Y-axis was cut to change scale and display large values. Statistical analysis was carried out using the Mann Whitney U. At least 260 ratios were calculated per treatment group from 4 separate experiments (**** p< 0.0001).

D) Frequency of new fired origins for *Mybl2*$^{+/+}$ and *Mybl2*$^{\Delta/\Delta}$ ESCs with or without ATM inhibitor treatment. Error bars represent SEM. Statistical analysis was carried out using unpaired t-test. At least 500 replication structures were counted per treatment group from 4 separate repeats.

E) Frequency of anaphases positive for UFB positive cells (based on ERCC/PICH positive immunostaining) *for Mybl2*$^{+/+}$, the *Mybl2*$^{\Delta/\Delta}$ and the *Mybl2*$^{+/+}$ treated for 2 hours with ATM inhibitor (KU60019). Data represents at least 100 anaphases from each group from 2 experimental repeats. Statistical analysis was performed using an unpaired two-tailed t-test.

F) Immunoblot showing the levels of phosphorylated ATM (Ser1987) and ATM in the *Mybl2*$^{+/+}$ and *Mybl2*$^{\Delta/\Delta}$ ESCs with or without CPT treatment (10µM CPT for 2 hours).

G) Distribution plot of replication speed in *Mybl2*$^{+/+}$and ATM$^{-/-}$ ESC treated or not for 90 minutes with 10µM KU60019 (ATMi), before sequential addition of IdU and CldU for 20 minutes each. Statistical analysis was carried out using the Mann Whitney U test. At least 200 replication forks were counted from 3 separate experiments for wild type and ATM$^{-/-}$ and two separate experiments for ATM$^{-/-}$ treated with ATM inhibitor . (**** p< 0.0001)

H) Quantification of the number of replication factories per cell for the different genotypes and treatments. A minimum of 65 early S-phase nuclei were counted per condition from two independent repeats. Statistical analysis was performed using a two-tailed unpaired unequal variance t-test.(**** p< 0.0001)

I) Distribution plot of replication speed in human iPSC and MEFs (primary and immortal). Statistical analysis was carried out using the Mann Whitney U test. At least 400 replication forks for iPSC,200 for primary MEFS and 250 for immortal MEFs were counted from 3 independent experiments. (**** p< 0.0001)

Figure 5. Replication speed phenotype in *Mybl2*$^{\Delta/\Delta}$ ESCs is epistatic with loss of MRE-11 nuclease activity.

A) Scheme of the procedure before DNA spreading. Cells were treated for 1.5 hours with 20uM MRe11 inhibitor (Mirin), before sequential addition of IdU and CldU for 20 minutes each.

B and C) Distribution curve of replication fork rates for *Mybl2*$^{+/+}$ and *Mybl2*$^{\Delta/\Delta}$ ESCs treated with mirin. Statistical analysis was performed using the Mann Whitney U test. n=3 experimental replicates. The value of the mean fork length is indicated above arrow (**** p< 0.0001)

D) Representative images of new firing origins, and elongating forks showing stable replication and fork instability.

E) Frequency of new firing origins (relative to total structures counted) from *Mybl2*$^{+/+}$ and *Mybl2*$^{\Delta/\Delta}$ ESCs treated or not with Mirin. At least 450 replication structures were counted per treatment from 3 independent repeats. Error bars represent SEM. Statistical analysis using two- tailed unpaired t-test.

F) Distribution and the average IdU/CldU ratio in *Mybl2*$^{+/+}$ and *Mybl2*$^{\Delta/\Delta}$ ESCs with or without MRE11 inhibitor treatment. The length of both incorporated labels for each elongating fork was measured in µm and the positive ratio was calculated. Percentage of highly unstable forks (ratio above 2) are indicated. Dotted line at 1 indicates positive ratio. Y-axis was cut to change scale and display large values. Statistical analysis was carried out using the Mann Whitney U test. At least 260 ratios were calculated per treatment group from 3 separate experiments.(**** p< 0.0001)

Figure 6. The replication defect observed after ATM inhibition and in *Mybl2*$^{\Delta/\Delta}$ ESCs is due to deregulation of cell cycle associated replication initiation control.

A, B) Scheme of the aim and procedure before DNA spreading. Cells were treated for 1.5 hours with ATM inhibitor (KU60019) or CDC7 inhibitor (PHA-767491) alone or in combination, before sequential addition of IdU and CldU for 20 minutes each.

C) Frequency of new firing origins (relative to total structures counted) from *Mybl2*$^{+/+}$ *and* *Mybl2*$^{\Delta/\Delta}$ ESCs treated or not with the indicated inhibitors: CDC7 inhibitor (PHA-767491) and/or ATM inhibitor (Ku60019). At least 300 replication structures were counted per treatment. Error bars represent SEM. Statistical analysis using two- tailed unpaired t-test (*p < 0.05).

D) Replication rate (kb/min) of *Mybl2*$^{+/+}$ and *Mybl2*$^{\Delta/\Delta}$ ESCs treated with the indicated inhibitors. Statistical analysis was carried out using an unpaired Mann Whitney U test (**** p< 0.0001). Minimum three independent experiments. At least 270 forks were scored for non-ATM inhibitor treated groups, and a minimum of 130 for ATM inhibitor treated groups.

E) Fork stability (average IdU/CldU ratio) of *Mybl2*$^{+/+}$ ESC and *Mybl2*$^{\Delta/\Delta}$ ESCs treated with the indicated inhibitors alone or in combination. At least 240 ratios were calculated for non-ATM inhibitor treated groups, and a minimm of 130 for ATM inhibitor treated groups. Y-axis was cut to change scale and display large values. Statistical analysis was carried out using Mann Whitney U test (**** p< 0.0001).

Data for *Mybl2*$^{+/+}$ ESCs treated with ATM inhibitor alone or in combination with CDC7 inhibitor, was collected from two independent experiments. For the rest of the conditions, a minimum of three independent repeats was performed.

F) Immunoblot showing the levels of CDC7 and actin in the *Mybl2*$^{+/+}$ and *Mybl2*$^{\Delta/\Delta}$ ESCs.

Figure 7. Schematic summary of our findings.

Expanded view Figure Legends

Figure EV1. Changes in the frequency of replication structures in *Mybl2*$^{\Delta/\Delta}$ *ESCs.*

A) Representative images of replication tracks from *Mybl2*$^{+/+}$*, Mybl2* $^{\Delta/\Delta}$ *ESCs.*

B) Representative images of new firing origins, and unstable elongating forks scored.

C-E): C) Frequency of elongating forks, D) Frequency of new firing origins and E) Frequency of first label only slowing/stalling events in *Mybl2*$^{+/+}$*, Mybl2* $^{\Delta/\Delta}$ ESCs calculated as a percent of all structures. Error bars represent SEM. Statistical analysis was carried out using two-tailed unpaired t-test. At least 1000 total structures were counted per condition, from 6 independent repeats.

Figure EV2. Proficent ATR activation in MYBL2-ablated ESCs.

A) Scheme of the procedure before DNA spreading. Cells were treated for 1.5 hours with 5uM ATR inhibitor (AZ20), before sequential addition of IdU and CldU for 20 minutes each.

B and C) Representative images of replication tracks from *Mybl2*$^{+/+}$, *Mybl2* $^{\Delta/\Delta}$ ESCs treated and untreated with ATRi. Scale bar 10um.

D) Representative images of new firing origins, and instability of elongating forks scored.

E) Distribution of replication fork rates for *Mybl2*$^{+/+}$, *Mybl2* $^{\Delta/\Delta}$ ESCs treated and untreated with ATR inhibitor AZ20 and ATMi KU66019. Statistical analysis was performed using the Mann Whitney U test (**** p< 0.0001). n=2 experimental replicates. A minimum of 100 replication forks were counted.

Figure EV3. MYBL2 deficiency and ATM inhibition do not alter the ESCs cell cycle.

Mybl2$^{+/+}$ and *Mybl2*$^{\Delta/\Delta}$ ESCs untreated and treated with ATM inhibitor (KU60019) for 2 hours were given BrdU (25uM) for the last hour of treatment. DNA synthesis and DNA content were assessed by flow cytometry. The proportion of the cells in the cell cycle was analysed using flowjo (untreated n=4; ATM inhibitor treated n=2 independent experiments). Error bars represent SD.

Figure EV4. Inhibition of ATM and MYBL2 deficency display similar number of replication factories and replication-associated genome instability.

A) Scheme of the experimental design.

B) Frequency of EdU positive cells showing more than six 53BP1 foci. At least 150 cells were counted per goup from 3 separate repeats. Error bars represent SEM. Statistical analysis using two-tailed unpaired t-test.

C) Representative images for *Mybl2*$^{+/+}$ and *Mybl2*$^{\Delta/\Delta}$ ESCs untreated and treated with ATM inhibitor (KU60019) taken at 40x magnification. DNA labelling (blue) EdU positive replicating cells (red) and 53BP1 (green). (Scale bar 10μm). Lower row shows merge staining. CPT treatment was used as positive control.

D) Representative rendering images of replication factories for the different genotypes and treatments after cells were cultured for 20 minutes in the presence of IdU. (Scale bar 5μm).

Figure EV5. Replication speed phenotype in *Mybl2*$^{\Delta/\Delta}$ ESCs is partially rescued by CDK1 and CDK1/2 inhibition.

A) Scheme of the aim and procedure before DNA spreading. Cells were treated for 1.5 hours with CDK1 inhibitor (RO3306),or ATM inhibitor (KU60019) alone or in combination, before sequential addition of IdU and CldU for 20 minutes each.

B) Frequency of new firing origins (relative to total structures counted) from *Mybl2*$^{+/+}$ *and* *Mybl2*$^{\Delta/\Delta}$ ESCs treated or not with the indicated inhibitors. At least 300 replication structures were counted per treatment. Error bars represent SEM. Statistical analysis using two- tailed unpaired t-test (ns= no significant).

C) Replication rate (kb/min) of Mybl2$^{+/+}$ and Mybl2$^{\Delta/\Delta}$ ESCs treated with the indicated inhibitors. Statistical analysis was carried out using an unpaired Mann Whitney U test (**** p< 0.0001. For non-ATMi treatmentst least 300 forks were scored from four independent experiments. A minimum of 130 forks were scored for ATM inhibitor treated groups. from two independent experiments .

D) Scheme of the aim and procedure before DNA spreading. Cells were treated for 1.5 hours with CDK1/2 inhibitor III or ATM inhibitor (KU60019) alone or in combination, before sequential addition of IdU and CldU for 20 minutes each.

E) Frequency of new firing origins (relative to total structures counted) from *Mybl2*$^{+/+}$ and *Mybl2*$^{\Delta/\Delta}$ ESCs treated or not with the indicated inhibitors. At least 200 replication structures were counted per treatmen from three independent experiments. Error bars represent SEM. Statistical analysis using two- tailed unpaired t-test (*p < 0.05; **p< 0.01; ns=no significant).

F) Replication rate (kb/min) of *Mybl2*$^{+/+}$ and *Mybl2*$^{\Delta/\Delta}$ ESCs treated with the indicated inhibitors. Statistical analysis was carried out using an unpaired Mann Whitney U test (***p< 0.001; **** p< 0.0001. A minimum of 130 forks were counted from three independent experiments. T.

G) Frequency of new origins (relative to total stuctures counted) and replication rate (kb/min) of Mybl2$^{+/+}$ ESCs treated with 3uM of CDK1/2 inhibitor III. (n=1). A total of 100 forks were counted. Statistical analysis using two- tailed unpaired t-test.

Methods

MYBL2 ablated mouse embryonic stem cells (mESCs) and ATM$^{-/-}$ ESCs generation and culture conditions.

New *Mybl2* $^{\Delta/\Delta}$ ESC, were generated from *Mybl2*$^{F/\Delta}$ mESCs (Garcia et al., 2005) following the same protocol as previously described (Lorvellec et al., 2010). *Atm*$^{-/-}$ ESC were derived from blastocysts generated from *Atm*$^{+/-}$ crosses as previously described (Lorvellec et al., 2010).

ESC were culture over mytomycin-treated MEFs feeder layer, using the media previously described (Ward et al., 2018). *Mybl2* $^{\Delta/\Delta}$ ESC used in all experiemnts were not grown past 15 passages. *Atm*$^{-/-}$ ESC were used before passage five. Cells were regularly tested for micosplasma contamination.

Inhibitors/Treatments

Cells were grown under different treatments as indicated in the figures. Colcemid Gibco, catalogue number 15212012; used at 0.27µM. Topoisomerase I inhibitor: Camptothecin (CPT), C9911, Sigma; used at 2.5-10µM. CDK1 inhibitor: RO3306, 4181, Tocris; used at 10µM. CDC7 inhibitor: PHA-767491, 3140, Tocris; used at 10µM. ATM inhibitor: KU60019, CAY17502-1, Cambridge bioscience; used at 10µM. ATR inhibitor: AZ20 5198, Tocris; used at 10µM. MRE-11 inhibitor: mirin M9948, Sigma; used at 20µM.

Western blotting

Western blotting was performed following standard procedures. Lysis buffer was previously described (Lorvellec et al., 2010). Primary antibodies: MYBL2 N19, sc724 (SCBT); P-CDK1 (Cdc2) (Tyr15), 10A11 (Cell signalling); CDK1, A17 (Boster); P-Chk1 (Ser345), 133D3 (CST); CHK1, Sc8408 (SCBT); GADPH, Ab8245 (Abcam); B-actin, Sc1616 (SCBT); ATM 2C1(Novus Biological); P-ATM (AF1655) GeneTex; CDC7, 3603 (Cell Signaling Techology).

DNA fibers

Exponentially growing cells were subject to various chemical inhibitors and stress inducing agents before labelling replicating DNA through incorporation of thymidine analogues in culture. During labelling, all media was pre-heated to 37^{o}C before adding to cells. Firstly, warm ESC media containing 30µM iododeoxyuridine (IdU) (I7125, Sigma) was added for 20 minutes. Cells were washed gently with warm media before addition of media containing 300µM chlorodeoxyuridine (CldU) (C6891, Sigma) for a further 20 minutes. Cell lysis and spreading and immunofluorescence was performed as previously described (Lorvellec et al., 2010), using Rat anti BrdU/CldU (ab6326) and Mouse anti BrdU/IdU (ab1816) both from Abcam. Imaging was carried out on a Leica DM6000 fluorescence microscope and images were taken at X60 magnification. Analysis of fibres was performed using the LasX software from Leica.

Replication factories

ESC colonies were exposed to experiment specific treatments before addition of 20µM IdU (I7125, Sigma) to the media for 20 minutes. Immunofluorescence wwas performed as previously described using a mouse anti-IdU antibody (Invitrogen, MD5000) (Lorvellec et al., 2010). Image acquisition was performed using a Zeiss LSM 780 confocal immunofluorescence microscope. During the early stages of S phase, the nucleus presents

numerous small foci throughout the nucleoplasm, whereas, in mid/late S phase cells, replication factories aggregate at the nuclear periphery before adopting a more clumped appearance (Dimitrova and Berezney, 2002; Ferreira and Carmo-Fonseca, 1997). Colonies containing early replicating cells were selected and z-stack images were acquired at 100X magnification with a distance of 0.4µm between each z slice. The images were then converted to 3D rendered projections using Imaris (x64.3.1) (Bitplane, Zurich, Switzerland). An automatic foci counting tool within the Imaris software was then used to automatically quantify the number of foci per cell. This was through the spots function in the surpass tool. Spots were defined as 'growing regions' with an estimated diameter of 0.3µm.

BrdU Flow cytometry

Cells were treated with 25uM BrdU for 1 hour and BrdU staining detected using FITC Mouse Anti- BrdU Set (BD Biosciences, 556028). Cells were resuspended in 10µg/ml 7-Amino-Actinomycin D (7-AAD) (BD biosciences, 559925) for the detection of DNA content. Analysis was performed using Flowjo.

Alkaline comet assays

$5x10^4$ ESCs were used per slide following the protocol previously described (Bayley et al., 2018).

Ultra-fine bridges

Experiment specific treatments were performed before washing cells with ice-cold PBS and fixation through treatment with 4% (v/v) PFA for 10 minutes. PFA was removed through PBS washes and formaldehyde groups were quenched through treatment with 50mM ammonium chloride for 10 minutes. Cells were washed three times more with PBS before adding ice-cold 100% methanol for 10 minutes. After repeating washes, cells were blocked in blocking buffer, 10% (v/v) FBS, 1% BSA (w/v) and 0.3% (v/v) Triton X in PBS, for 1 hour at room temperature. Antibody staining was performed using an anti-ERCC6 primary antibody (H00054821, Abnova), 1 in 100 in blocking buffer at 4^oC overnight, and an anti-rabbit Alexa 488 secondary antibody (A31565, Thermo Fisher) at 1 in 500 in blocking for 1 hour at room temperature. Slides were mounted in prolong plus DAPI before storing at -20^oC. Microscopy was performed using a Leica DM6000 fluorescence microscope; anaphase cells were visualised by DAPI staining and the percentage of anaphases with ultra-fine bridges was determined for each sample.

Immunofluorescences

Cells were fixed in 4% paraformaldehyde for 20 minutes before washing twice in PBS. Permeabilization and blocking was carried out through treatment with blocking buffer containing 1% (w/v) BSA and 0.3% (v/v) triton X in PBS for 1 hour at room temperature. Cells were then incubated with a mouse anti-H3-pS10 (9701S) primary antibody at a

concentration of 1 in 200 in blocking buffer at 4^{o}C overnight or a rabbit anti-53BP1 primary antibody (Novus Biologicals NB100-304) at 1 in 500 in blocking buffer at 4^{o}C overnight. A separate slide was also incubated with an anti-mouse IgG antibody (Santa-cruz, sc2025) or rabbit IgG (sc-2027, Santa Cruz) for an IgG control. Slides were washed twice in PBS before incubating with goat anti-mouse Alexa 488 secondary or anti-rabbit Alexa 488 secondary antibody (A31565, Thermo Fisher). Imaging was performed using a Leica DM6000 fluorescence microscope and images were taken at x40 magnification for 53BP1 staining or at 20x magnification for H3-pSer10 staining. The number of 53BP1 foci per nuclei/ pr positive nuclei for H3-P-Ser10 was counted manually using the counting plugin for Image J.

For detection of H3-pSer10, prior to fixation, ESCs were treated with 2.5µM CPT for 4 hours; 0.1ug/ml (0.27µM) colcemid was added for the final 3.5 hours to arrest cells which pass into mitosis. Cells were immediately harvested on ice before washing in PBS and centrifugation at 250g for 5 minutes at 4^{o}C. 5x10^{4} cells were cytospun at 300g for 5 minutes onto microscope slides and air dried for 15 minutes.

For detection of 53BP1 foci, 10µM EdU (C10337, Thermo fisher) was added to cells in culture for 1 hour before harvesting on ice and a click-IT recation, and a “click” reaction was performed after fixation and permeabilization prior to antibody staining.

Detection of EdU through a Click reaction

Staining of incorporated EdU was performed through a ‘click’ reaction representing the reaction between an alkyne (conjugated to EdU) and an azide (fluorescently labelled). A reaction cocktail was made containing 86% Tris buffered saline (TBS) (50 mM Tris-Cl, pH 7.5, 150 mM NaCl), 4% (v/v) 100mM $CuSO_4$, 0.125% (v/v) Alexa-fluor azide 594 (C10330, Thermo Fisher) and 10% (v/v) 1M sodium ascorbate added in the order presented. 200µl of the reaction cocktail was added to each slide under a cover slip and incubated for 30 minutes in the dark. Slides were washed several times in PBS before re-blocking for 30 minutes in blocking solution.

Figure 1

A

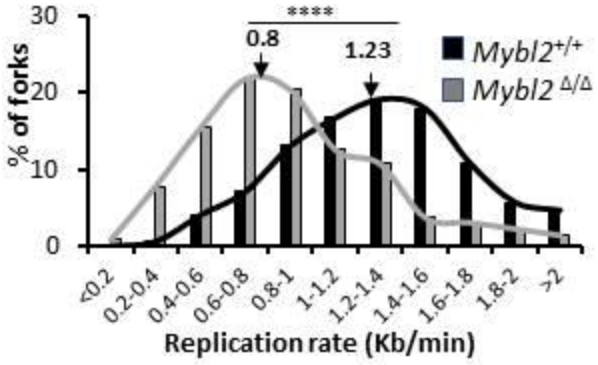

E

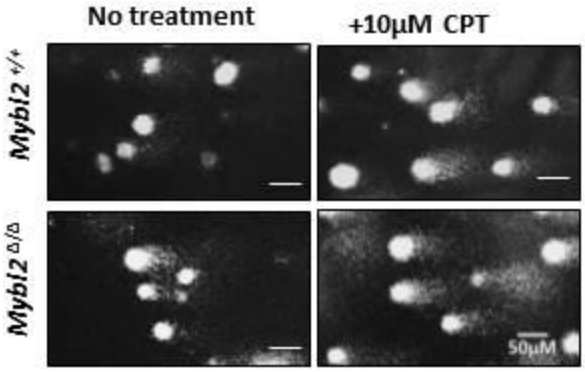

B

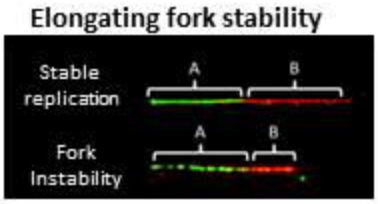

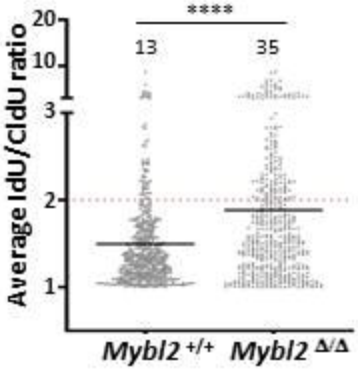

F

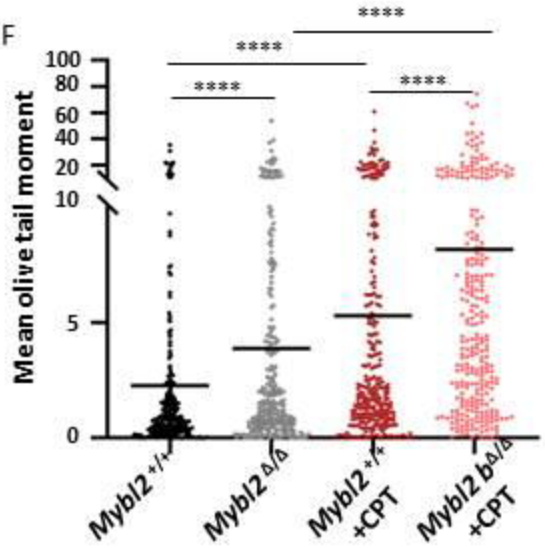

C

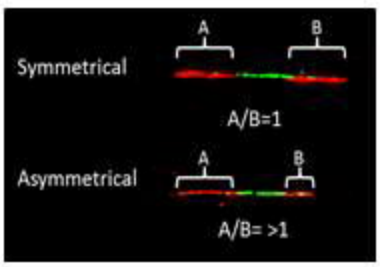

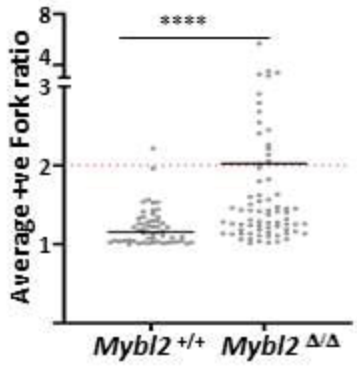

G

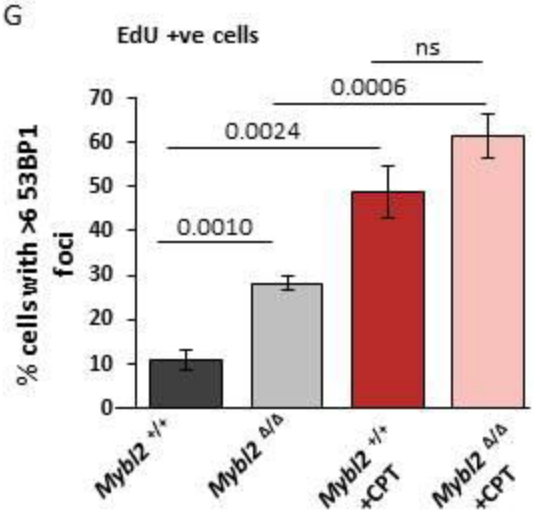

D

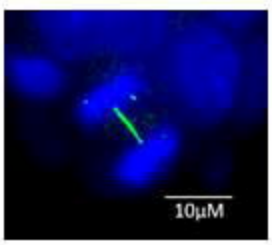

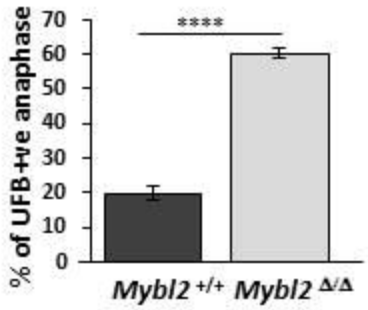

Figure 2

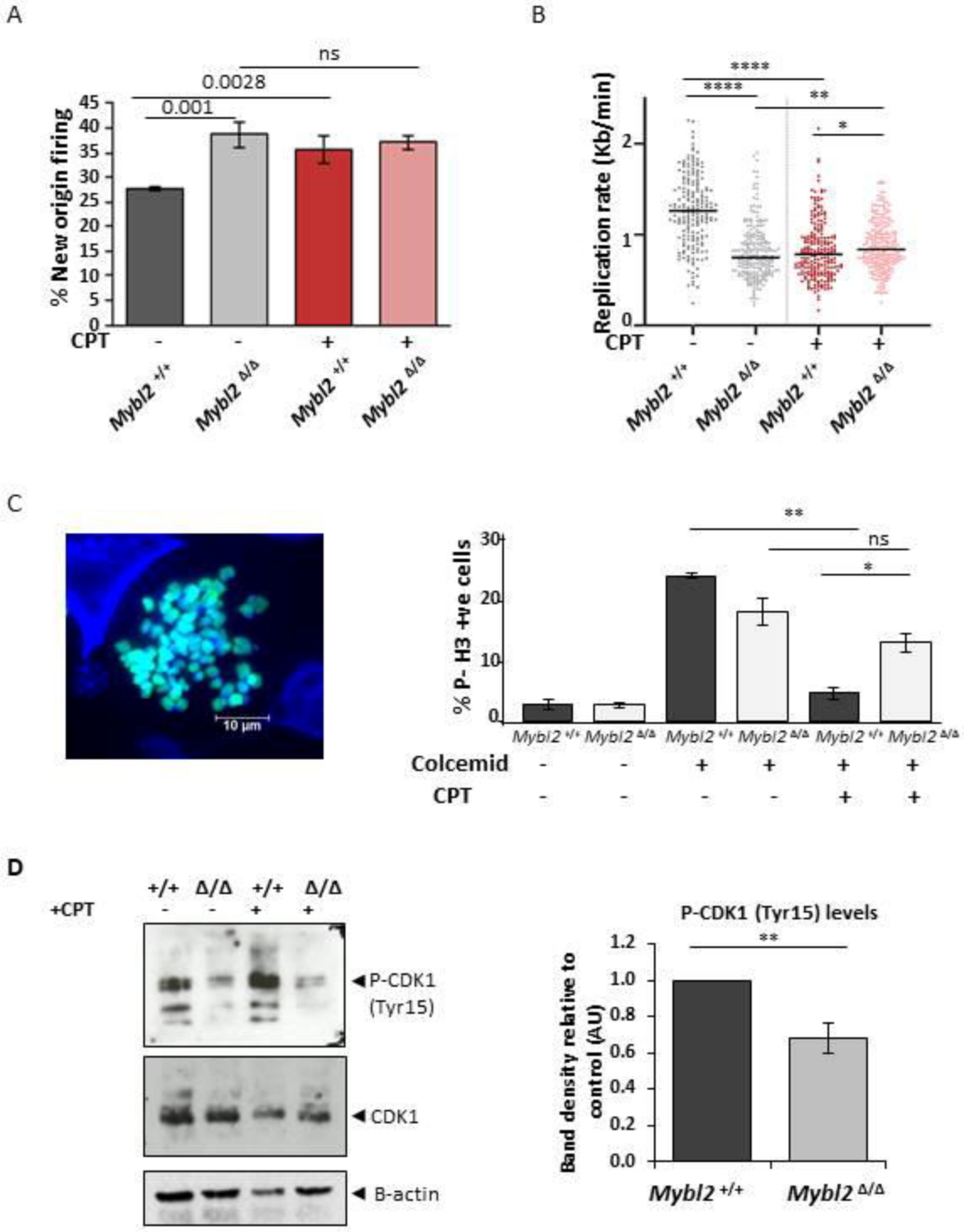

Figure 3

A

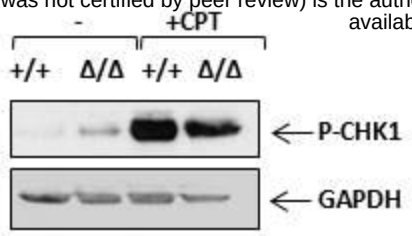

B

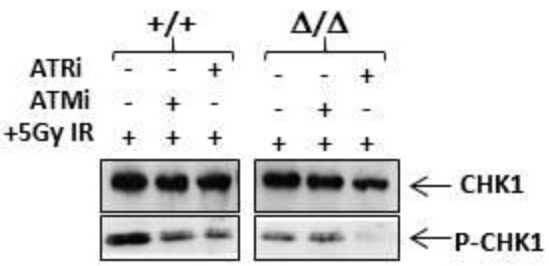

D

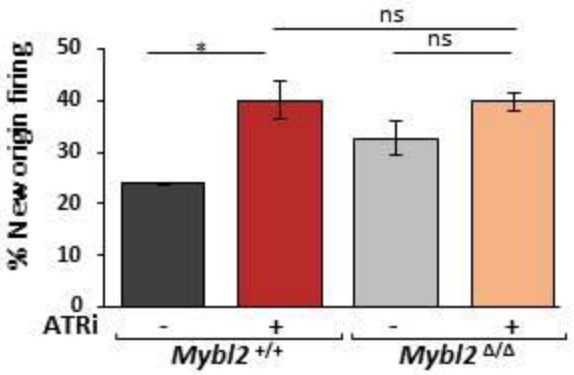

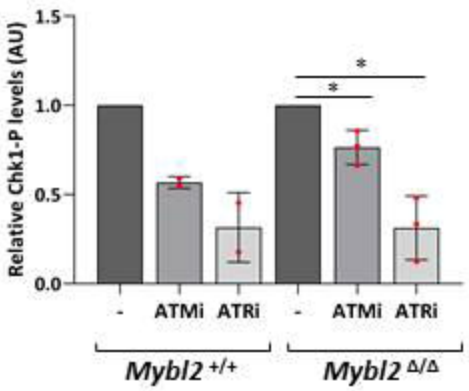

E

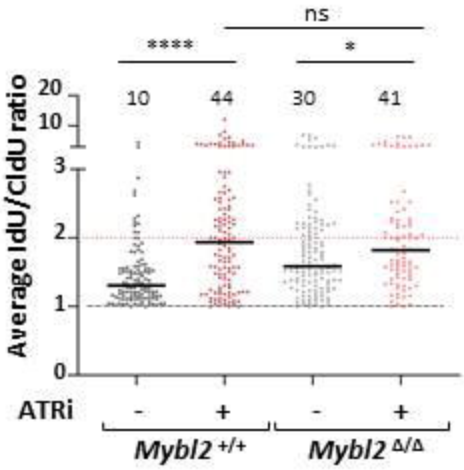

C

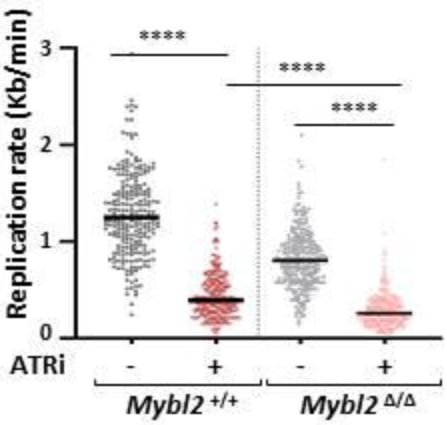

FIGURE 4

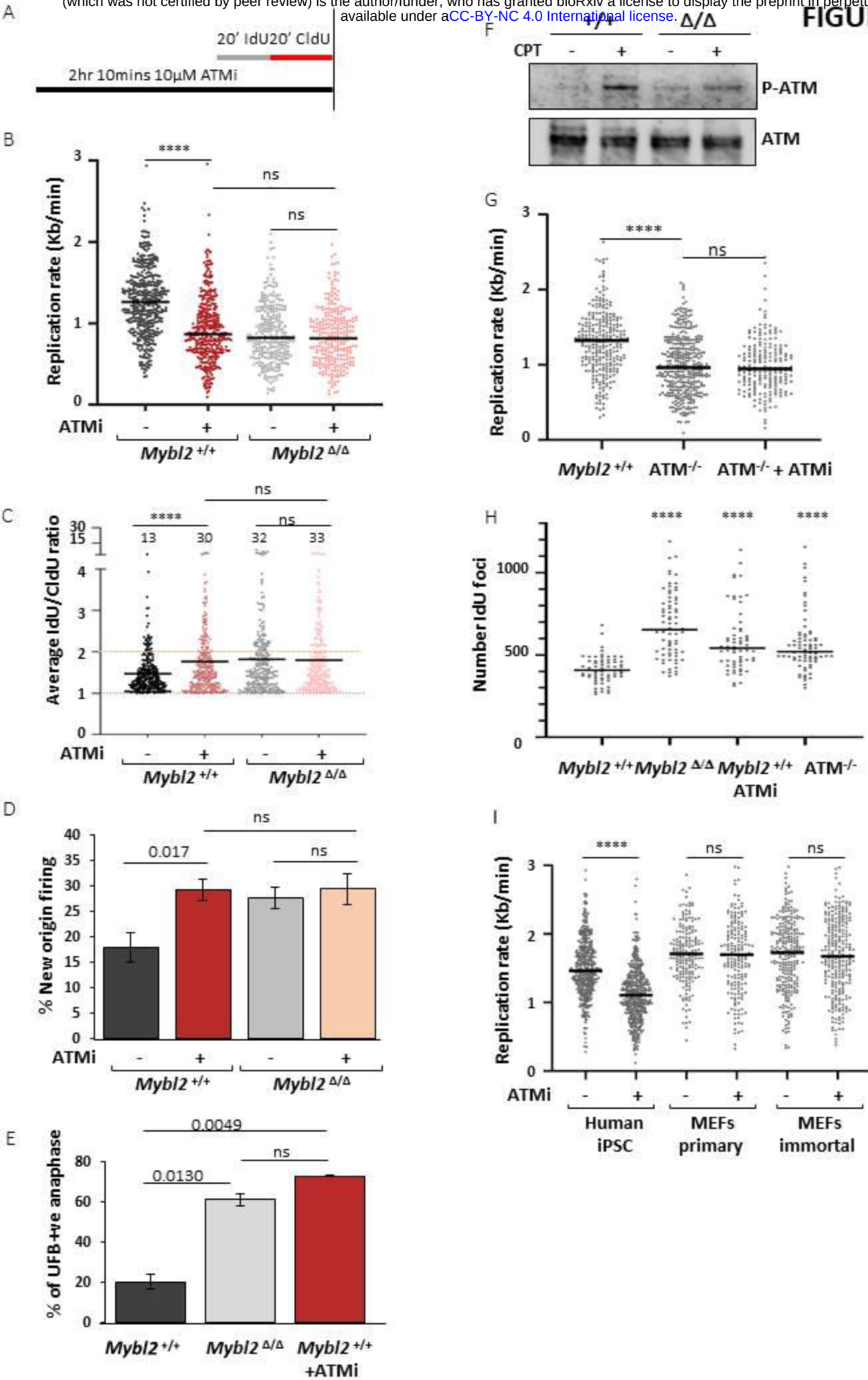

Figure 5

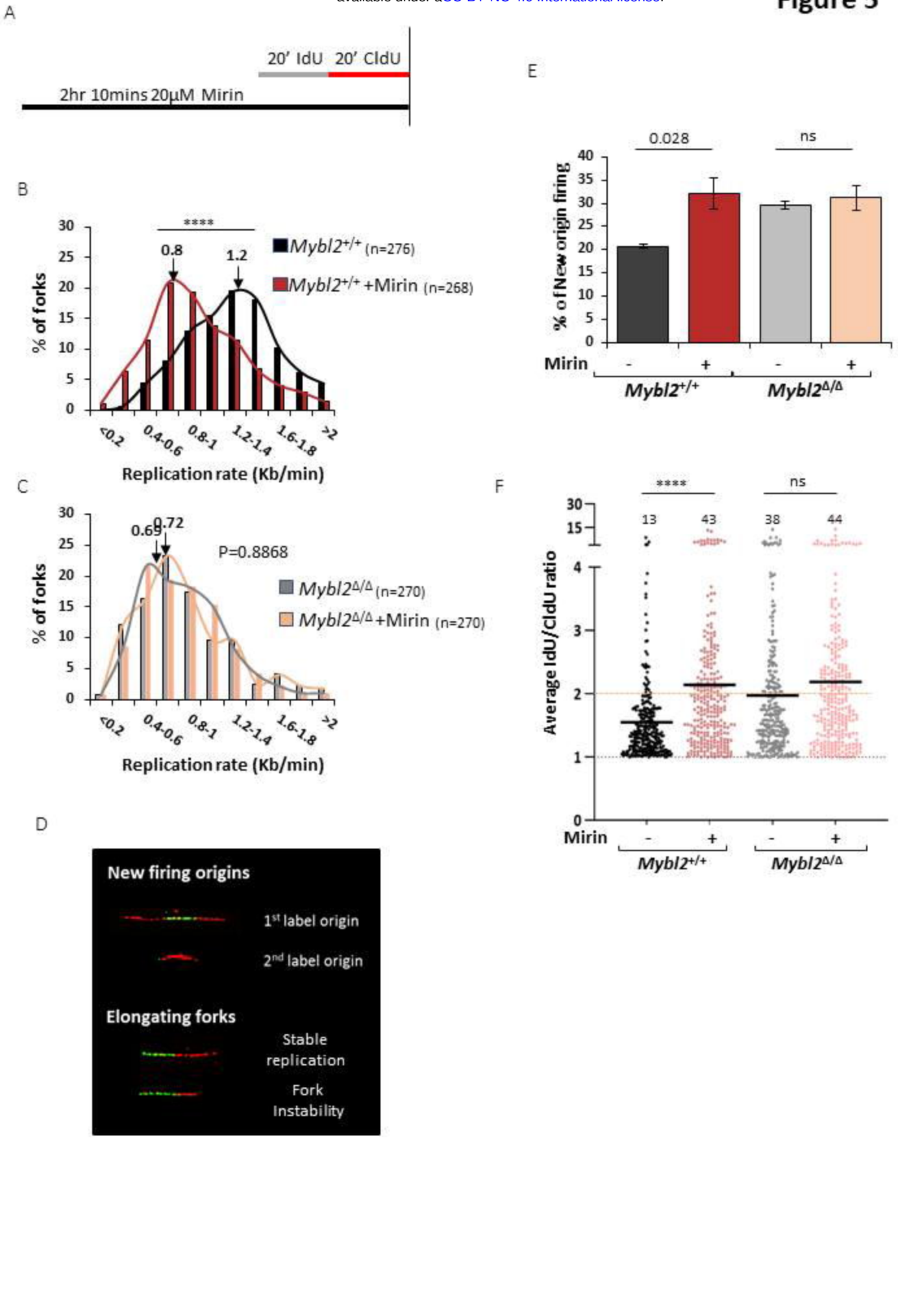

Figure 6

A

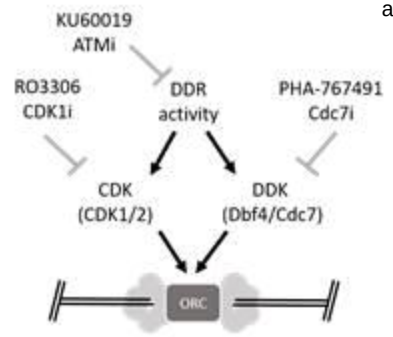

B

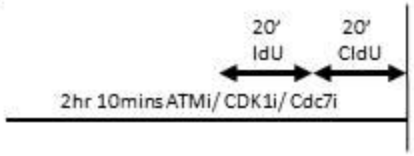

C

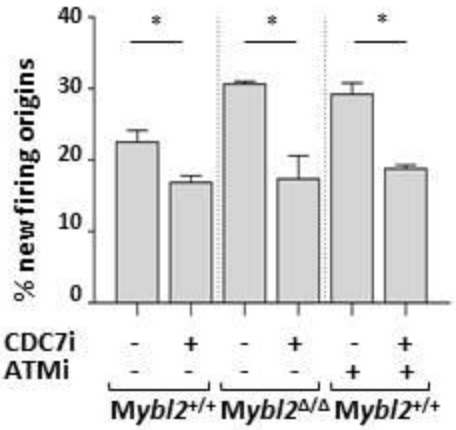

D

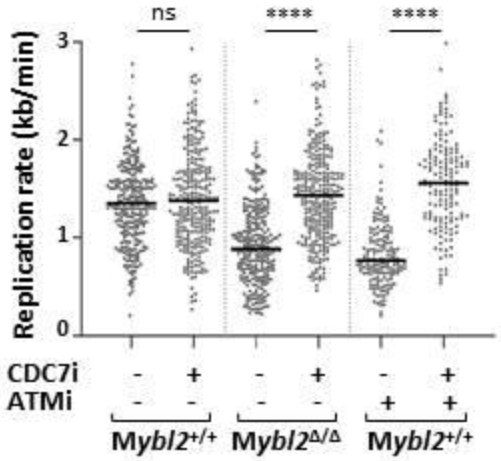

E

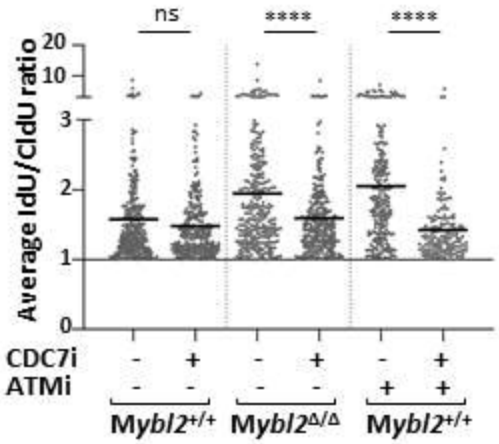

F

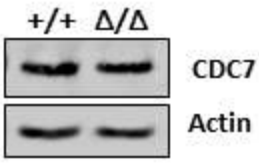

Figure 7